

Numerical and Experimental Methods for Estimating the Propagation Loss in Microphotonic Waveguides

Francesco Dell'Olio,* Samuel M. Hörmann, Teresa Natale, Roel Baets, and Alexander Bergmann

The accurate estimation of propagation loss in microphotonic waveguides is a crucial factor in the performance optimization of photonic integrated circuits. This article presents a comprehensive review of both numerical and experimental methods used to estimate propagation loss. Numerical methods, including volume current, finite-difference time domain, finite element, and eigenmode expansion, offer high precision by modeling the intrinsic physical characteristics of waveguides, such as sidewall roughness, which significantly contributes to scattering loss. However, these methods are heavily dependent on detailed physical measurements, including roughness profiles. In contrast, experimental approaches like the cut-back method and interferometric techniques provide practical means for measuring propagation loss in real-world settings. These methods, while simpler and faster, are limited in their capacity to explain the origins of propagation loss. The synergy between numerical and experimental techniques is critical to developing effective strategies for minimizing loss in advanced photonic integrated circuits. The findings of this study highlight the necessity for continuous improvement in both computational and experimental methods to enhance the performance of microphotonic waveguides.

sciences, robotics, and automotive,^[5,11–18] it holds great potential, with ongoing research paving the way for future advancements. The pivotal role these advancements play in enabling cutting-edge systems underscores their significance in the technological landscape.


The increase in PIC complexity highlights a growing demand for innovative solutions that address the challenges posed by the miniaturization and integration of photonic components. Dielectric waveguides serve as the backbone of these circuits, enabling the precise control and manipulation of light within a compact footprint. As the quintessential building block of PICs, the dielectric waveguide's performance is crucial, influencing the overall functionality and efficiency of the integrated system. Therefore, getting a reliable and efficient estimation of how much propagation loss there is in these waveguides becomes very important for designing, optimizing, and testing PICs.

1. Introduction

The emergence of the concept of integrated photonics and the subsequent exponential growth in terms of the complexity of photonic integrated circuits (PICs) have marked a paradigm shift in the photonics realm over the last few decades.^[1–5] This transformative wave, which began with the integration of just a few components on a single chip^[6] and now allows for very complex PICs with hundreds of thousands of components,^[7,8] has revolutionized transceivers for telecommunication and data communication.^[9,10] In other fields such as aerospace, defense, life

In the pursuit of technological advancement, the predominant platform for PIC development is the silicon-based one that exploits silicon-on-insulator wafers. Its high index-contrast enables the realization of compact, high-performance photonic circuits. On the other hand, the silicon-based platform cannot always support all the features that advanced applications need. This generates a growing interest towards heterogeneous PICs.^[19–23] These innovative circuits combine components consisting of different materials, such as silicon, silicon nitride, III-V semiconductors and lithium niobate, on a common wafer, most often a silicon wafer. The development of very innovative

F. Dell'Olio, T. Natale
Micro Nano Sensor Group
Department of Electrical and Information Engineering
Polytechnic University of Bari
70125 Bari, Italy
E-mail: francesco.dellolio@poliba.it

 The ORCID identification number(s) for the author(s) of this article can be found under <https://doi.org/10.1002/adpr.202500103>.

© 2025 The Author(s). Advanced Photonics Research published by Wiley-VCH GmbH. This is an open access article under the terms of the Creative Commons Attribution License, which permits use, distribution and reproduction in any medium, provided the original work is properly cited.

DOI: 10.1002/adpr.202500103

S. M. Hörmann, A. Bergmann
Institute of Electrical Measurement and Sensor Systems
Graz University of Technology
8010 Graz, Austria

S. M. Hörmann
ams OSRAM Group
Tobelbader Strasse 30, 8141 Premstaetten, Austria

R. Baets
Photonics Research Group
Department of Information Technology
Ghent University
9052 Ghent, Belgium

technology platforms, such as the lithium niobate-on-insulator one or those combining ultralow-loss silicon nitride waveguides and III-V semiconductors, not only broadens the functional capabilities of PICs but also introduces new challenges and opportunities in propagation loss optimization.^[24]

There are many different types of waveguide structures used in PICs and integrated photonic components. Strip and rib waveguides with silicon or silicon nitride cores^[25,26] and ultralow-loss waveguides with silicon nitride cores^[27,28] are among the most widely used. All of these waveguides are fabricated starting from either silicon-on-insulator or bulk silicon wafers. In standard strip or rib configurations, the underlying oxide layer is typically a few micrometers thick. The top silicon or silicon nitride layer, with a thickness in the 200 nm to 600 nm range, is fully or partially etched to form the waveguide. Typical waveguide widths range from about 400 nm to 1000 nm. The ultralow-loss waveguide is realized by first depositing a thick oxide layer—on the order of 10 μm —onto a bulk silicon wafer. A very thin silicon nitride layer (about 100 nm thick) is then deposited on top of this oxide and patterned, usually with waveguide widths of several micrometers. Finally, an additional oxide layer is deposited over the patterned waveguide. The diversity of these guiding structures reflects the evolving needs of integrated photonics, where the quest for reduced losses and enhanced performance is relentless. These waveguides, with cross section as shown in **Figure 1**, are among the most studied in terms of propagation loss. Their typical loss value ranges from a few dB cm^{-1} to a few dB m^{-1} and they represent useful examples to discuss the numerical and experimental techniques for assessing the dielectric waveguides propagation loss.

The performance of particular integrated photonic devices depends almost exclusively on the loss suffered from the waveguide itself. Integrated photonic resonators, such as ring resonators, are directly limited in their Q-factor and performance by the propagation loss of the waveguide.^[29–31] In addition, for quantum key distribution applications, the waveguide loss is one of the most critical design parameters.^[32] For these kinds of devices, getting an accurate estimation of the waveguide propagation loss is important both for design and for finding a physical interpretation based on optical characterization results.

This review article delves into the experimental and numerical methodologies that have been developed to estimate propagation losses in dielectric waveguides within the domain of integrated photonics. The complexity of PICs and the multifaceted nature of

their components necessitate a sophisticated approach to loss estimation, one that can accommodate the interplay between material properties, waveguide geometry, and optical behavior. Numerical methods offer a powerful tool for theoretical analysis, enabling the simulation of waveguide performance under a variety of conditions and configurations. These computational approaches provide invaluable insights into the mechanisms of light propagation and loss in dielectric waveguides, facilitating the optimization of waveguide design and material selection in the early stages of PIC development. Conversely, experimental methodologies play a crucial role in the assessment of waveguide performance, offering a measure of propagation losses under real-world conditions. The synergy between numerical simulations and experimental measurements is essential, as it allows for the validation of theoretical models and the refinement of design parameters based on experimental data. The evolution of experimental techniques, ranging from cut-back methods to sophisticated interferometric and resonator-based approaches, reflects the ongoing quest for accuracy, sensitivity, and reliability in the characterization of photonic components.

Estimating propagation losses in dielectric waveguides is a complex challenge that is critical in the field of integrated photonics. Moving forward with PICs, making them faster and more integrated, the methods for estimating loss must also get better. This will make the design and optimization of next-generation photonic circuits more accurate, efficient, and flexible. This review aims to provide a comprehensive overview of the state-of-the-art in loss estimation techniques, highlighting their key contributions, limitations, and potential pathways for future research. Through this analysis, we endeavor to shed light on the critical role of propagation loss estimation in the advancement of integrated photonics, paving the way for the development of more efficient, compact, and functional photonic devices.

1.1. Definitions and Physical Sources of Loss

In the optical characterization of waveguides, distinguishing between insertion loss and propagation loss often presents a challenge. Insertion loss refers to the comprehensive loss incurred when a waveguide or device is integrated into a system. This loss includes both the loss within the PIC and from coupling it off-chip. Conversely, propagation loss pertains to the loss

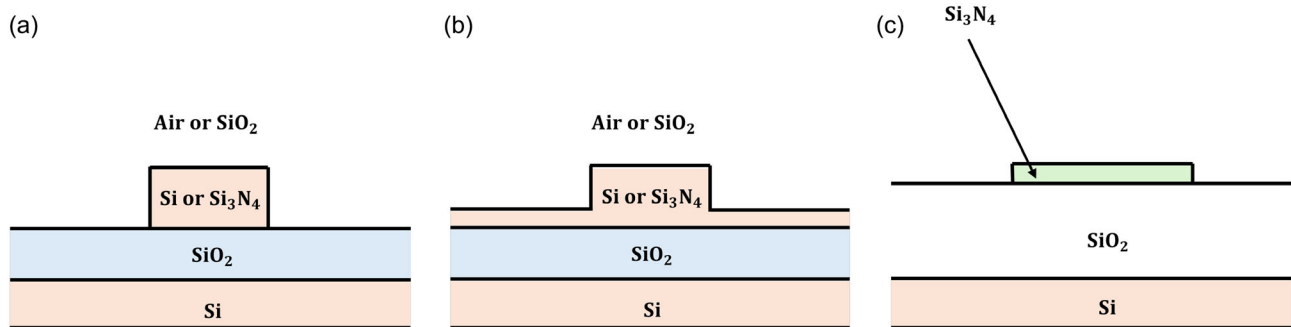


Figure 1. Cross section of three typical waveguides widely utilized in silicon photonics and PICs. a) Silicon or silicon nitride strip waveguide. b) Silicon or silicon nitride rib waveguide. c) Silicon nitride ultralow-loss thin strip waveguide.

that occurs as a result of transmission within the waveguide, specifically excluding coupling losses. During the development or research phase aimed at enhancing device performance, focus typically shifts towards minimizing propagation loss. This is because the factors contributing to this type of loss, such as the design of the waveguide or the properties of the materials used, are crucial for improvement.

The sources of propagation loss in photonic waveguides primarily include 1) scattering and backscattering loss attributed to sidewall roughness, which often represents the most significant source of loss; 2) linear absorption loss resulting from metal near the guiding structure or from material absorption, which is usually small in materials like undoped silicon, silicon oxide, and silicon nitride within their transparency windows but can reach dB/cm levels or more in doped silicon or other nontransparent materials; 3) nonlinear absorption loss due to two-photon absorption, which occurs in semiconductors whenever the photon energy exceeds half the bandgap and which can become dominant as a loss mechanism at high power levels; 4) leakage towards the substrate; and 5) bending loss, which depends on the curvature radius of bent waveguides.^[33] As will be discussed in Section 2, the latter three sources of loss can be accurately calculated using state-of-the-art full-vectorial mode solvers. However, accurately numerically estimating scattering loss proves to be more challenging.

The rest of this article is organized as follows. The numerical methods for propagation loss estimation are discussed in Section 2. The experimental methods for loss estimation are presented in Section 3. In Section 4, a conclusion is drawn.

2. Numerical Methods

Propagation loss has a large impact on the design. All of its above-mentioned sources, i.e., absorption, surface-roughness-induced scattering, backscattering, leakage, and radiation, may contribute significantly in a particular device or circuit. From a design perspective, analytical solutions are preferable because fundamental dependencies are apparent and the consequences of choosing a specific waveguide platform may be immediately deduced. Perturbation theory enables the calculation of the contributions to the propagation loss from expressions containing solely the guided modes of the ideal structure. Thereby, useful scaling laws and dependencies are established, often explicitly. Furthermore, the required computational effort is significantly reduced allowing for integration in simulation suites. For simple geometries that feature known analytical solutions for the electromagnetic fields of the modes, i.e., the slab waveguide and the cylindrical fiber, analytical expressions may be achieved through approximations.

On the other hand, the massive computing power currently available allows for the ubiquitous application of numerical methods from simulation suites during the design phase. In general, the computational treatment of optical waveguides is well established^[34,35] and an integral part of a typical design workflow.^[36] Finite-difference time domain (FDTD),^[37,38] finite element (FE),^[39,40] eigenmode expansion (EME),^[41] and beam propagation method (BPM)^[42] are the prevalent mesh-based methods in 3D problems.^[43] They are typically used in

conjunction with perfectly matched layers (PMLs) to emulate an infinite simulation domain.^[44] Alternatively, spectral methods may be utilized.^[45–47] 2D methods allow the eigenmodes of a given waveguide cross section to be determined in a reduced setting.^[48–50] These numerical approaches are of primary interest for the topics discussed herein because they serve as an efficient basis for perturbation theory that utilizes the mode fields. Advanced structures and approaches benefit from optimized techniques.^[51,52]

Because of these methods, both semianalytical and fully numerical approaches that rely on perturbation theory and the unperturbed guided modes are on hand for the calculation of all loss contributions. Indeed, it is already possible to set up simulations in which the nanometer scale of roughness is resolved to directly compute the scattering loss.^[53] Hence, analytical approximations, semianalytical models, and purely numerical methods all may be integrated into a design flow in integrated photonics. Therefore, the matter at hand is about striking a balance between accuracy, time and effort, and simplicity. In this section, we will set the available methods into context to enable an informed decision. We will consider the modeling of propagation loss in longitudinally invariant, i.e., straight, waveguides that feature guided modes, and also waveguide discontinuities and bends. The interested reader is referred to corresponding models and assessments regarding photonic crystal (PhC) waveguides.^[54,55]

We will treat surface-roughness-induced scattering in Section 2.1, absorption in Section 2.2, backscattering in Section 2.3, and leakage in Section 2.4. The handling of waveguide discontinuities and bends is described in Section 2.5 and 2.6. The topic of surface roughness analysis crucial for modeling surface-roughness-induced scattering is discussed in Section 2.7. Finally, we will exemplarily show the computed propagation loss in two representative strip waveguides in Section 2.8. The first insightful platform is a SOI platform operated at 1550 nm, where we investigate the surface-roughness-induced scattering at the sidewalls. Because datacom is currently the largest market in integrated photonics,^[8] similar platforms are currently in use in the majority of integrated photonic devices. Due to the high refractive index contrast in SOI and vanishing absorption, devices with low loss and a very small footprint may be designed.^[56] The second useful case is a silicon nitride platform operated at 850 nm due to its transparency down to the visible spectrum.^[57] We apply a unified perturbative treatment considering sidewall-roughness-induced scattering of all waveguide interfaces, absorption, and radiation. Based on observations of qualitative behavior common to both, we will derive general properties of the impact of the waveguide geometry and present design guidelines in Section 2.8.3.

2.1. Surface-Roughness-Induced Scattering

Modeling of surface-roughness-induced scattering rests upon the distinction of the intrinsically loss-less guided modes, which usually carry the signal of interest, and the power-dissipating radiation modes.^[58,59] Perturbing the ideal system couples both types of modes and power is drained from the guided modes. Furthermore, some of the power is redistributed among the guided modes, leading to cross coupling and reflection. To

determine the corresponding attenuation coefficient is therefore a matter of modeling both the perturbation and the total coupled power. In this section, the available models will be discussed. A summary is tabulated in **Table 1**.

2.1.1. Perturbation Theory

Models of surface-roughness-induced scattering relying on perturbation theory contain the roughness characteristics and the known guided modes, because the perturbed modes are described as superposition of the unperturbed ones.^[58] The surface roughness is represented as a perturbation in the permittivity of the waveguide system

$$\epsilon'(\mathbf{r}) = \epsilon(\mathbf{r}) + \Delta\epsilon(\mathbf{r}) \quad (1)$$

where $\mathbf{r} = (x, y, z)$ is the coordinate. Traditional perturbation theory puts the perturbation in ϵ that impacts the modes in relation to a causative quantity ξ through

$$\Delta\epsilon(\mathbf{r}) = \frac{\partial\epsilon}{\partial\xi}(\mathbf{r})\Delta\xi(\mathbf{r}) \quad (2)$$

Translating Equation 2 to the surface roughness results in the first expression for a shift Δh in a material interface

$$\Delta\epsilon(\mathbf{r}) = (\epsilon_1 - \epsilon_2)\Delta h(\mathbf{r}) \quad (3)$$

with the permittivities ϵ_i of the materials. The magnitude of the shift Δh at (\mathbf{r}) defines the rough interface and was described as a stochastic process through its autocovariance function.^[60] However, Equation 3 may cause incorrect results due to a discontinuity in the expression

$$\Delta\epsilon\epsilon \quad (4)$$

when multiplied with the mode's (unperturbed) electric field \mathbf{e} .^[61] The effect is especially pronounced in high-refractive-index-contrast systems. Therefore, a framework containing entirely continuous components of Equation 4 with a well-defined expression was devised by smoothing the discontinuous component through a harmonic mean,^[62] resulting in an effective tensor for the perturbation

$$\Delta\epsilon(\mathbf{r})\mathbf{e}(x, y) = \begin{pmatrix} \frac{\epsilon_1 - \epsilon_2}{\epsilon_1 \epsilon_2} \epsilon^2(\mathbf{r}) & 0 & 0 \\ 0 & \epsilon_1 - \epsilon_2 & 0 \\ 0 & 0 & \epsilon_1 - \epsilon_2 \end{pmatrix} \mathbf{e}(x, y) \Delta h(\mathbf{r}) \quad (5)$$

for an interface with its (unperturbed) normal oriented in the direction of x and for mode propagation in z . ϵ_1 and ϵ_2 are the permittivities of the waveguide and the cladding, respectively.

The first inquiries into the mechanisms of scattering considered slab waveguides^[60] and cylindrical fibers,^[63] for which guided and radiation modes of the ideal system may be analytically determined and coupled mode theory (CMT) may be applied.^[60,63,64] Even for these simple geometries, however, this procedure results in a complicated integral over the radiation modes. Roughness further induces cross coupling between guided modes, which may be similarly considered within CMT.^[58,65–67]

However, strip and rib waveguides are more common.^[35] Unfortunately, these profiles do not allow for an analytical determination of the mode fields.^[2,68] Hence, CMT cannot be directly applied. Fortunately, systems with small refractive index contrast

Table 1. Comparison of various models of surface-roughness-induced scattering. Class denotes the broader category: VCM assumes free-space radiation modes, improved VCM (IVCM) approximates the true radiation modes and integrates the radiated power, CMT computes the true radiation modes and coupled power, and FDTD numerically simulates the radiation. Geometry classifies the cross sectional shape. Mode is the allowed mode. Dim. is the dimensionality of the surface roughness. Autocov. is the incorporated autocovariance of the surface roughness. Perturb. is the type of perturbation. Cont. specifies whether the model features a perturbation that is continuous across the waveguide interfaces that scatter. Effort is the computational effort.

Reference	Class	Geometry	Mode	Dim.	Autocov.	Perturb.	Cont.	Effort
Payne and Lacey (PL) ^[78]	VCM	SLAB	Even + odd TE	1D	Exponential, Gaussian	Scalar	No	Low
Yap et al. ^[91]	VCM	slab	Even + odd TE	1D	Exponential, Gaussian	Scalar	No	Low
Melati et al. ^[94]	Regression	Arbitrary	–	None	None	None	–	Low
Peng et al. (PLP) ^[96]	VCM	Slab	Even + odd TE	1D	Exponential	Scalar	No	Low
Zadehgoi ^[90]	VCM	Slab	Even TE	1D	Exponential	Scalar	No	Low
Barwicz and Haus ^[75]	IVCM	Slab	TE, TM	1D	Exponential	Scalar	No	Low
Schmid ^[76]	IVCM	Slab	TE0, TM0	1D	Exponential	Tensor	Yes	Low
Poulton et al. ^[98]	CMT	Arbitrary	Arbitrary	1D	Arbitrary	Tensor	No	Low
Ciminelli et al. ^[112]	VCM	Arbitrary	Arbitrary	1D	Exponential	Scalar	No	Low
Ciminelli et al. ^[79]	IVCM	Arbitrary	Arbitrary	1D	Exponential	Scalar	No	High
Hörmann et al. ^[114]	VCM	Arbitrary	Arbitrary	2D	Arbitrary	Tensor	Yes	Low
Jabaransary et al. ^[53]	FDTD	Arbitrary	Arbitrary	2D	Gaussian iso/aniso/mix	Exact	NA	High
Zhang et al. ^[119]	FDTD	Arbitrary	Arbitrary	2D	Gaussian iso	Exact	NA	High
Guiana and Zadehgoi ^[77]	FDTD	Slab	Arbitrary	1D	exponential	Exact	NA	Medium
Kita et al. ^[120]	FDTD	Arbitrary	Arbitrary	1D	none	Tensor	Yes	High

allow for a truncation in the dyadic Green's function and the radiation modes may be approximated by the free-space modes.^[69–71] Therefore, the perturbations in the permittivity may be treated as imaginary currents, or equivalently, radiating dipole sources.^[72,73] Consequently, antenna theory may be consulted and the scattered power is obtained by simply integrating over the resulting far field. This approach is known as the volume current method (VCM).

Lacey and Payne applied VCM to derive the scattering caused by striations at the interfaces of a symmetrical slab waveguide system.^[74] They approximate the appearing integrals to investigate the relation of the scattered field on the roughness' autocovariance, obtaining a superposition of cylindrical waves. In their nonapproximated VCM expression, they retain flexibility in the autocovariance's form. They numerically compare the impact of exponential and Gaussian autocovariances to CMT^[60] over a range of waveguide thickness and observe good agreement. It has been remarked that in their formula a factor of 2 appears to be missing.^[75–77] Payne and Lacey (PL model) take it further and condense the estimate by approximating the integrals through the method of steepest descent for the TE₀ mode and the two cases of both previously investigated autocovariances.^[78] They further insert the explicitly known fields of the symmetric slab waveguide and obtain an analytical estimation of the scattering coefficient within VCM. Hence, the impact of normalized waveguide parameters in the slab waveguide system are readily accessible. They also corrected the previously missing factor of 2. They propose to employ their model also for 3D waveguide systems by ways of the effective refractive index method. A claim against which the argument was brought forward that using the solutions in a 2D system misrepresents the radiation modes in the 3D case and cannot capture the true dependencies on waveguide parameters.^[75] Further, it was postulated to overestimate the propagation loss of 3D waveguides.^[55,75] Even for a low-index system, applying the 2D model to strip waveguides may induce a significant error.^[79] While the qualitative behavior of their theory has doubtlessly proven to be extremely useful, it had trouble making quantitative predictions in several instances^[80–83] and the bespoke overestimation was observed in many cases.^[84–87] On the other hand, adequate agreement was achieved for high aspect ratio waveguides.^[27,88,89] However, inconsistencies in the formulation of the electric field and power in the PL model have been noted.^[90]

Yap et al. affixed a correction factor to the PL formula to account for the overlap of the electric field with the scattering surfaces in 3D waveguides.^[91] However, they prescind from the electric field at the sidewall and instead use the derivative of the modes' effective refractive index with regard to the rib width, which perturbation theory uncovers as a measure of the field strength at the sidewall interface.^[59,92,93] Melati et al. took this idea further to recast the PL formula for the sidewall roughness induced scattering entirely in terms of a contribution of the roughness and the effective refractive index's derivative with regard to the slab width.^[55,94] Further, they introduce an analogous term accounting for contribution of the top and bottom roughness based on the effective refractive index method.^[2] The high level of abstraction enables the application also to 3D structures. They further reduce backscattering to a similar expression, creating a unified perception (see Section 2.3).

They numerically fit the remaining factors containing the roughness to measured propagation losses. A similar concept supported by a modified effective refractive index method^[95] was introduced by Peng et al. (PLP model).^[96] They include the scattering due to the top and surface roughness while retaining the PL formula. They apply their approach to a trapezoid waveguide.

As explained by Zadehghol,^[90] the expression for the electric field in PL model was adapted from Adams^[97] and assumes both even and odd TE modes propagating in the slab waveguide. Therefore, Zadehghol utilizes a corrected formulation resting upon VCM that captures a single even TE mode.^[90] Combined with the approach to solve the angular integral over the roughness' spectrum via the residue theorem instead of the previous approximation, Zadehghol obtains an analytical expression which shows improved accuracy for large correlation lengths compared to the PL model. However, Guiana and Zadehghol note that the addressed formula depends on the optical power.^[77] To rectify this unwanted dependency, they heuristically affix a correction factor and compare the implied optical power which is necessary for good agreement with the previous work of PL model. They point out that this discrepancy is due to the normalization of the electric field implied by the work of Lacey and Payne,^[74] which leads to incorrect results when omitted. They verify their results through FDTD simulations discussed in Section 2.1.3.

At this point, it is important to highlight that the issue encountered in high-refractive-index-contrast platforms for the above models is twofold. First, the radiation modes do not correspond well to the free-space modes.^[71,98] Therefore, the power coupled into them cannot be estimated within the radiating antenna framework without quantitative error. Second, the formulation of the perturbation as in Equation 3 was inconsistent because of the discontinuity in the electric field at the material junction,^[61] a problem later solved^[62] through the consistent perturbation from Equation 5 and applied in some of the semianalytical models in Section 2.1.2. By extension, the perturbation was made applicable to guiding-wave systems with arbitrary refractive index profiles. However, the first problem remains.

2.1.2. Semianalytical Models

As eluded, the advent of ubiquitous computing power has enabled the incorporation of more numerical simulations. Hence, the guided modes of arbitrary waveguide cross sections are easily attainable and more realistic radiation modes can be computed. Some methods slightly improve the VCM by approximating the true radiation modes using the free-space radiation modes of reduced systems.^[99–101]

Often, the dimensionality of the problem is reduced by assuming 1D striations in the roughness. In the case of sidewalls, which are the dominant sources of the dominant sidewall-roughness-induced scattering of 3D waveguides, vertical striations are typically adopted. This allows for the direct evaluation of the integral over the corresponding dimension.

Barwicz and Haus (BH model) expanded the dyadic Green's function, representing a symmetric slab waveguide as derived by Chew et al.,^[102] to leading order.^[75] Thus, they improved the incorporated radiation modes because they account for multiple

reflections in the layered medium. The physical interpretation is that they differentiate between the scattering from the roughness directly into the cladding and the portion that is transmitted through the slab's 2 interfaces to the other side. Thereby, they prescind towards CMT yet improve upon VCM, which assumes that the radiation is scattered into plane waves in a homogeneous medium around the individual sources. They further use 1D surface roughness and they average the results from both sides of the field discontinuity at the interfaces. Having addressed both issues of high-refractive-index-contrast systems, they claim that their model is applicable universally. However, the complexity of the used Green's function necessitates numerical calculation. A further approximation of keeping their dyadic Green's function for slab waveguides also for 3D waveguide systems makes their model truly versatile.^[85] They justify this approximation of the strip waveguide's radiation modes by the small angular cross sectional area in which the strip system is different from the slab system, as experienced from the scattering sources' point of view. However, quantification of the resulting error is not provided. Therefore, depending on the unknown Green's function of the particular rectangular waveguide system at hand, the model may be less representative than the simpler VCM. As pointed out,^[79] this approximation implies that the approach is not fully 3D. Yet, the higher the aspect ratio of a strip waveguide, the more accurate the BH model approximates the real system. Furthermore, they approximate the electric field distribution at the rough interface by a constant through normalization in order to get manageable expressions.

Similarly, Schmid et al. used a different formulation of the Green's function of a layered medium,^[76] posed by Sipe.^[103] A detailed comparison of the relevant formulations can be found in.^[104] Analogous to the PL model, they approximated the integrals using the steepest descent method. Thus, they arrive at integral expressions of the scattering coefficients of the TE₀ and TM₀ modes. By solving the integrals containing the transmission and reflection coefficients and the spectral density of the roughness, analytic expressions may be obtained. They use a tensor as perturbation that is continuous over the interface.^[105] Finally, they compare their model to the PL-model and to experimental values for 3D SOI waveguides. In the latter trial, they observe moderate quantitative discrepancies, but the qualitative behavior w.r.t. waveguide thickness.

Poulton et al. numerically determined the radiation modes in a strip waveguide within a homogeneous cladding material in order to apply CMT.^[98] They start with the coupled-mode equations^[58,93]

$$\pm \frac{dc_\mu}{dz}(z) = -i \sum_\mu [\kappa_{\mu\nu}^t(z) + \kappa_{\mu\nu}^z(z)] e^{i(\beta_\mu - \beta_\nu)z} c_\nu(z) \quad (6)$$

with the amplitude coefficients c_μ of mode μ , and the coupling coefficients $\kappa_{\mu\nu}^t$ between modes μ and ν , where

$$\kappa_{\mu\nu}^t(z) = \frac{\omega}{4\sqrt{P_\mu P_\nu}} \int_A \Delta\epsilon(\mathbf{r}) \mathbf{e}_{\mu t}(z) \cdot \mathbf{e}_{\nu t}^*(z) dx dy \quad (7)$$

$$\kappa_{\mu\nu}^z(z) = \frac{\omega}{4\sqrt{P_\mu P_\nu}} \int_A \frac{\epsilon(\mathbf{r})\Delta\epsilon(\mathbf{r})}{\epsilon(\mathbf{r}) + \Delta\epsilon(\mathbf{r})} e_{\mu z}(z) e_{\nu z}^*(z) dx dy \quad (8)$$

and

$$P_\mu = \frac{1}{2} \Re \left[\int_A (\mathbf{e}_\mu(x, y) \times \mathbf{h}_\mu^*(x, y)) \cdot \hat{\mathbf{z}} dx dy \right] \quad (9)$$

P_μ is the transported power in the cross sectional area A and its unit normal $\hat{\mathbf{z}}$, and $\mathbf{e}_{\mu t}$, $\mathbf{e}_{\mu z}$ are the transversal and longitudinal components of the electric field of mode μ , respectively. They apply the approximation of weak coupling that allows them to directly obtain a solution to Equation 6 coupled Mode after further assuming that only one mode μ is excited at $z = 0$. Finally, they integrate over the continuum of radiation modes and sum over the populated guided modes to get the power attenuation

$$2\alpha = \sum_\nu \int_{-k}^k |\kappa_{\mu\nu}^t + \kappa_{\mu\nu}^z|^2 S(\beta_\mu - \beta_\nu) \frac{|\beta_\nu|}{\rho} d\beta_\nu \quad (10)$$

Under the above assumptions, the coupling coefficients in Equation 7 only depend on z through the perturbation $\Delta\epsilon(\mathbf{r})$. Hence, it was factored out and integrated. As a result, the roughness's characteristics is included through its spectrum S that may be calculated from the autocovariance κ through

$$\pi S(q) = \frac{1}{2} \int_{-\infty}^{\infty} d\Delta z \kappa(\Delta z) e^{iq\Delta z} \quad (11)$$

Thus far, their derivation followed.^[58] In order to find the fields of the radiation modes and evaluate Equation 7, they develop a method to account for the presence of the waveguide in the calculation of the radiation modes and radiation loss for arbitrary refractive index contrast. To this end, they extended an approach previously developed for the computation of the guided modes of a strip waveguide.^[106] They expand the radiation modes' z -component in terms of cylindrical harmonics (see Figure 2). They compared a radiation mode accounting for the presence of the waveguide with its free-space counterpart (see Figure 3). They highlight that the difference is more pronounced for lower order modes and in the waveguide's vicinity. However, this subtlety is important for quantitatively computing the coupling into the radiation modes: First, the coupling is determined by the overlap of the radiation modes with the perturbation at the waveguide's interface, and second, the contribution of lower-order modes to the radiation loss dominates. According to their model, they predict lower and wider waveguides would exhibit smaller losses. These configurations simultaneously reduce the contributing sidewall area and increase the propagation coefficient. They compared their model for varying correlation length to the 2D model for a slab waveguide,^[60] the VCM with free-space radiation modes, and FDTD simulations. They showed that for such a square waveguide, the 2D model is inaccurate, although the qualitative behavior is retained. The VCM improves the prediction but still underestimates the scattering for low and medium correlation lengths. At higher correlation lengths, the VCM matches the FDTD simulations actually better than the CMT. Although their expression includes a tensor perturbation, it is not of the same form as in Equation 5.^[62] Instead, it stems from a modal expansion in the transverse components of the electric and the H-field (a 4-vector) in CMT.^[65,107,108] By contrast, the other models discussed herein rely on modal expansion in

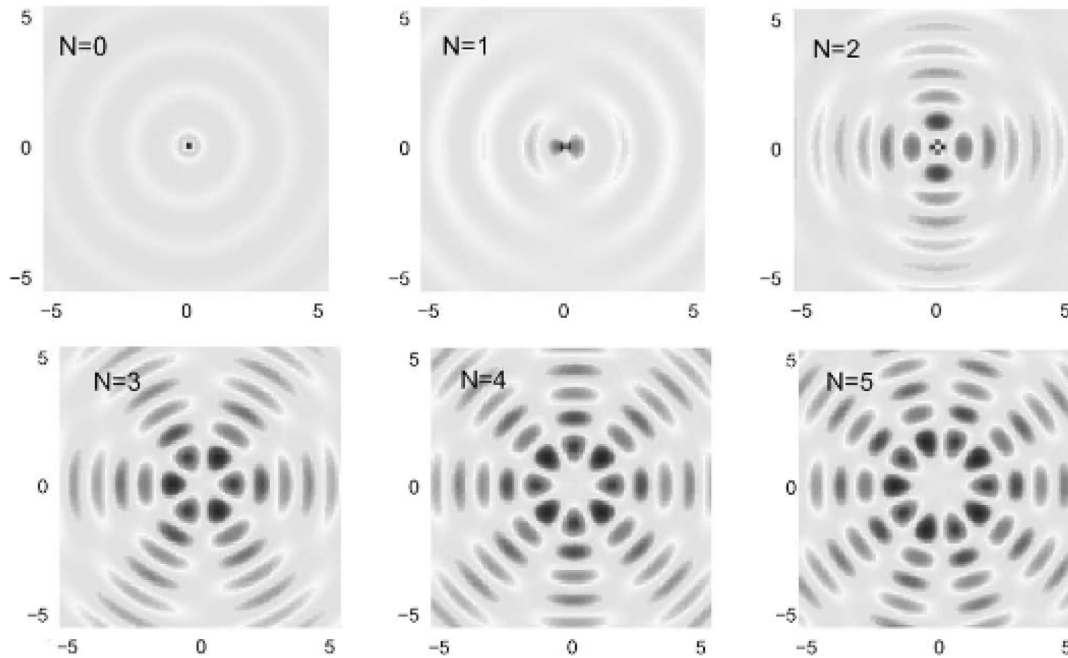


Figure 2. Numerically computed radiation modes of a square silicon waveguide in vacuum. They correspond to cylindrical harmonics with far-field order N and serve as an expansion basis for numerically computing the true radiation modes. Reproduced with permission.^[98] Copyright 2006, IEEE.

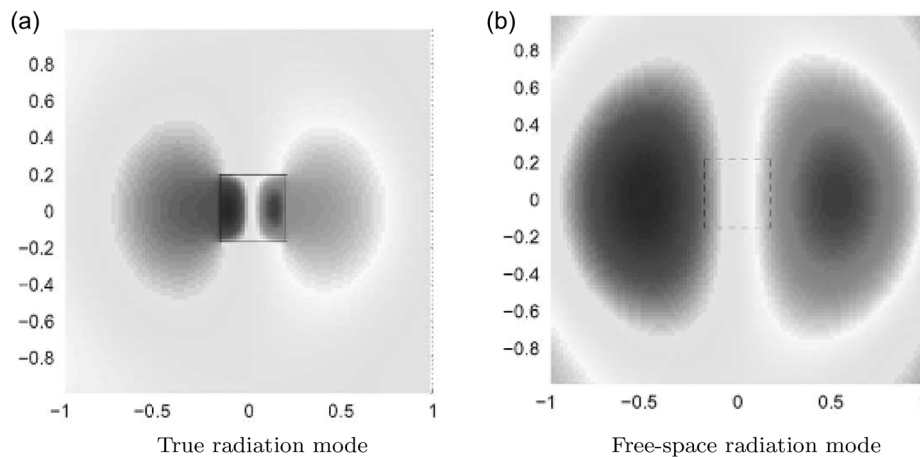


Figure 3. a) Comparison of the true and b) the free-space radiation mode in a square silicon waveguide in vacuum. The presence of the waveguide perturbs the true mode which can be accounted for through an expansion in cylindrical harmonics. Reproduced with permission.^[98] Copyright 2006, IEEE.

the 3D electric field,^[109] which induces an error of $\mathcal{O}((\Delta\epsilon)^2)$.^[110] However, the discontinuity in the perturbation at the waveguide surface owing to the use of the original expression persists. Therefore, they had to model two separate contributions depending on the sign of the perturbation, effectively building the mean. Finally, they fabricated InGaAsP strip waveguides on an InP pedestal, measured the sidewall roughness using an AFM, applied their model, and compared the results with the measured propagation loss values determined using the cut-back method. They considered only the z-component of the autocovariance function.

They observed harmonic oscillations combined with an expected decay in the sample autocovariance (SAC) function. The traditional exponential autocovariance function achieved a satisfactory fit in terms of LMSE. They applied their model based on these values and obtained predictions which agree within the uncertainties with the experimentally measured values.

Papakonstantino et al. introduced an analogous concept to multimode waveguides.^[111] They postulate an efficient algorithm for the numerical computation of the radiation modes and apply CMT to estimate the scattering coefficient in the modal

equilibrium distribution, as derived by Marcuse.^[58] They find that the assumed 1D roughness uncouples odd and even modes, and hence, two equilibria form.

Ciminelli et al. allow for the 3D radiation mode fields to be included directly in a semianalytical manner.^[112] Thus, the 2D approximation relying on the fields^[78] or the radiation modes^[75] of a slab waveguide was removed. They relied on the original perturbation expression^[60,72] and the assumption of vertical striations to derive an integral expression for the scattering coefficient in small-refractive-index-contrast platforms. They retain full flexibility with regard to the polarization and modal field distribution. Hence, they investigate the dependency of the scattering loss on the radius in bent strip waveguides on a $\text{In}_{0.75}\text{Ga}_{0.25}\text{As}_{0.55}\text{P}_{0.45}/\text{InP}$ platform by computing and inserting the distorted mode fields of the bent platform via a 3D simulation. Further, they compare the estimation of their model to experimentally measured values in the investigated low-index-contrast system.^[113] Bauters et al. apply this method to estimate the bend loss by reducing the bent waveguide to an effective straight waveguide.^[27] Ciminelli et al. point out that fully numerical techniques are better suited for high-index-contrast systems. Therefore, they expanded their method with a 3D FEM simulation of the radiation (modes) for the case of high index-contrast.^[79] Thereby, they obtained a highly accurate model that estimates the measured propagation losses from diverse high-index-contrast systems with relative errors lower than 3%. By circumventing the estimation of the radiation modes via their numerical component, they make their model applicable to arbitrary waveguide systems. Yet, this CMT approach comes at the cost of increased computational effort.

Hörmann et al. relied on VCM and Gaussian processes to devise a 3D formalism that allows for the roughness' 2D spectral properties to be fully captured.^[114] Similarly to Ciminelli et al.,^[112] their model is semianalytical and includes the unperturbed mode's fields directly. Furthermore, they utilize the consistent perturbation from Equation 5 devised by Johnson et al.^[62] Considering a sidewall surface located at x_0 with a normal in \hat{x} , the field attenuation coefficient α is calculated according to the VCM through an integration over the azimuthal ϕ and inclination θ angles

$$2\alpha = \frac{1}{P} \int_0^\pi d\theta \sin(\theta) \int_0^{2\pi} d\phi u(\theta, \phi) \quad (12)$$

of the radiation intensity

$$u(\theta, \phi) = \frac{\mu_0 \omega^4}{32\pi^2 c_0} \pi S_z(\beta - k_z) \int_0^H d\gamma \times \int_0^H d\gamma' \kappa_\gamma(\gamma - \gamma') o(\theta, \phi, \gamma, \gamma') e^{-ik_\gamma(\gamma - \gamma')} \quad (13)$$

where ω is the angular frequency, μ_0 is the vacuum permeability, c_0 is the vacuum speed of light, and k is the wavevector in the cladding assuming plane waves. o is an overlap coefficient that contains the mode's electric fields

$$o(\theta, \phi, \gamma, \gamma') = \begin{pmatrix} \frac{\epsilon_1 - \epsilon_2}{\epsilon_1 \epsilon_2} \epsilon^2(x_0, \gamma) e_x(x_0, \gamma) \\ (\epsilon_1 - \epsilon_2) e_y(x_0, \gamma) \\ (\epsilon_1 - \epsilon_2) e_z(x_0, \gamma) \end{pmatrix} \cdot \hat{T}(\theta, \phi) \begin{pmatrix} \frac{\epsilon_1 - \epsilon_2}{\epsilon_1 \epsilon_2} \epsilon^2(x_0, \gamma') e_x^*(x_0, \gamma') \\ (\epsilon_1 - \epsilon_2) e_y^*(x_0, \gamma') \\ (\epsilon_1 - \epsilon_2) e_z^*(x_0, \gamma') \end{pmatrix} \quad (14)$$

which are transformed into spherical coordinates by \hat{T} . The 2D nature of the roughness is captured by including both κ_γ and S_z . The components must be adapted depending on the orientation of the surface under consideration. They compare their estimates with the modified PL model by Yap et al.,^[78,91] the Barwicz and Haus model,^[75] and CMT.^[98] They find it showed higher accuracy than the (partly 2D) VCM approaches, comparable to CMT. However, extremely high compliance as the model from Ciminelli et al.^[79] could not be achieved. Nevertheless, as a VCM approach their model is computationally efficient and large parameter spaces may be easily computed. Exploiting this advantage, they utilized their model to optimize a polarimetric and a bimodal waveguide interferometer on a silicon nitride platform for biosensing.^[115,116] The dependency of the total propagation loss, i.e., comprising scattering from all surfaces, absorption, and radiation, on the curvature radius of a bent strip waveguide were investigated by Hinum-Wagner et al.^[117] However, even though the issue regarding the discontinuity of the perturbation expression was resolved, the model still approximates the radiation modes of the system as the free-space modes.^[114] Therefore, further evidence is necessary to determine the quantitative error inflicted by the VCM approach with increasing refractive index contrast between core and cladding. Moreover, they point out that the higher complexity of the fully 2D roughness was insufficiently investigated and experimental data is lacking. This issue is discussed in Section 2.7. Hence, their comparison with experimental values from literature investigates which correlation length leads to most accurate predictions. The dependency on the correlation lengths of an anisotropic exponential autocovariance was analyzed. In contradiction to the assumption of vertical striations in the previous models, a significant dependency was observed on both parameters and even setting the y correlation length to finite values that are larger than the waveguide height instead of infinity are not to be neglected. Along the waveguide length, a critical value of the z correlation length was found when the roughness oscillates in unison with the mode. This connection was established using the Gaussian process framework. The occurrence of a critical correlation length in a 2D slab waveguide was explained by Zadehgo.^[90] By contrast, increasing the y correlation length leads to higher scattering because this further assimilates roughness and mode behavior.^[114] A similar version of the model was derived independently for modelling propagation loss in hollow-core fibers.^[118]

Another problem that is difficult to treat through the VCM is the estimation of the reflected power coupled into other guided modes, including reflection. However, for a single-mode silicon waveguide with square cross section, it was found that the dominating contribution is the radiation loss.^[98] This is because the

reflected modes have a higher difference in the propagation coefficient than the radiation modes. Therefore, their coupling is reduced.

2.1.3. Fully Numerical Methods

Entirely numerical methods to estimate the propagation loss necessitate the modelling and simulation of the (sub-) nanometer scale roughness features. Hence, the challenge lies in finding appropriate adaptive or anisotropic meshes that can still be computed with reasonable effort. Furthermore, the simulations need to be fully 3D to capture the nature of the directional characteristics and the field profiles. However, these approaches have the advantage that nonparametric roughness values as estimated by methods relying on the periodogram or the SAC function might be directly integrated in future endeavors.

Jaberansary et al. model the surface roughness directly in 3D-FDTD simulations and observe the scattering from boundary effects.^[53] They generate surfaces with a 2D Gaussian autocovariance function by filtering in the spectral domain. They employ three different autocovariance functions to investigate the anisotropy of the sidewall roughness and its impact: isotropic, anisotropic, and a mixed composite. Compared to the PL model, they improve accuracy to an experimentally measured value for one low-aspect-ratio waveguide.

Zhang et al. model the surface roughness by filtering in the spectral domain and apply the generated 2D surface to the sidewalls of a ring resonator in a 3D FDTD simulation.^[119] They use an isotropic Gaussian autocovariance function. They investigate the distortions of the mode profile depending on the correlation length, which also leads to increasing asymmetric fields. Further, they compare the results to the PLP model over the correlation length. Note that owing to the used isotropic autocovariance, a compound effect between the different characteristics of the scattering loss with respect to the correlation lengths along the waveguide length and height arises.^[114] The 2D characteristics of the roughness makes comparison with the PL model difficult, since it assumes a 1D roughness, even with the PLP modification. They simulate the transmission of the ring resonator to compare the spectrum with the experimental one and find reasonable agreement of the Q-factor, even though measurement and fit uncertainties are not given.

Guiana and Zadehghol generate exponentially correlated 1D surfaces and set up a 2D symmetrical slab waveguide in a FDTD simulation that evaluates the scattering loss by monitoring the mode's transmission through the rough section.^[77] Their estimation for the investigated SOI slab agrees with the PL model, but the BH model deviates. They also compare measured propagation losses from 3D SOI waveguides, but a 1:1 comparison is not possible.

Kita et al. utilize FDTD simulations to estimate the scattering loss coefficient and optimize the waveguide geometry in sensing applications.^[120] To this end, they first numerically investigate the polarizability of the roughness, i.e., the dependency of the imaginary current sources' magnitude on the unperturbed field. They find that the surface shift may be assumed flat if the correlation length of the assumed Gaussian autocovariance is much larger than the root mean square (RMS) value. They also use the

improved perturbation from Johnson et al.^[121] Second, they simulate the radiated and backscattered power caused by 1D line sources in a 3D FDTD setup. Third, they obtain the total power loss by averaging over the waveguide length. Because of their approximations and their relative comparison, they are able to completely neglect the spectral characteristics of the surface roughness. This is the decisive difference to the method from Ciminelli et al.^[79] Finally, they combine the computed loss values with sensitivities to bulk and surface permittivity changes in a figure of merit to assess and compare the waveguide structures. They find that structures with low confinement lead to increased scattering for the same reason they possess high sensitivities: higher overlap with the perturbation. Because the limit of detection of an integrated photonic sensor ultimately depends on the transmitted power as well, the advantages are largely negated.

2.2. Absorption

In state-of-the-art integrated photonic systems, the loss is minimized by choosing and optimizing the materials carefully through advanced fabrication techniques.^[122,123] In this case, the imaginary part of the materials' permittivity is negligible in the simulations. Subsequently, the absorption and its attenuation coefficient can be calculated using perturbation theory because the materials may be treated as weakly absorbing.^[93] Because the modal fields' dependency on a perturbation in the permittivity is of second order, whereas the propagation coefficient's dependency is of first-order,^[124,125] the attenuation coefficient is calculated from the unperturbed fields. To this end, the perturbation is included as in Equation 1, and the power attenuation is calculated through an overlap integral^[126]

$$2\alpha = \frac{\omega}{2P} \int_A \Delta\epsilon(x, y) |e(x, y)|^2 dx dy \quad (15)$$

However, if there are materials with permittivities whose imaginary part is comparable to or exceeds their real part, e.g., metals,^[127] the attenuation needs to be computed in one sweep with the propagation coefficient and the modal fields.

2.3. Backscattering

In a similar way to out-of-plane radiation, any permittivity perturbation of the ideal waveguide structure leads to a fraction of the power in the forward propagating mode to be coupled into the backward propagating mode, and vice versa.^[128] Regarding the propagation loss in imperfect waveguides, it has been observed that the contribution of backscattering is only a fraction of the surface-roughness-induced scattering loss.^[129,130] Nevertheless, it was argued by Morichetti et al. that the backscattering may impede achieving ultralow-loss waveguides.^[129] However, it is commonly accepted that both backscattering and out-of-plane scattering due to surface roughness scale with the square of the RMS value of the surface roughness. Hence, out-of-plane scattering will predominate over backscattering independent of the improvement, unless the roughness' spectral characteristics or the modes' propagation coefficient change in such a way that the spectral bands contributing to the respective scattering cause a distinct impact. However, predominating

backscattering has not been observed to the best of our knowledge. Nevertheless, backscattered light can cause additional disturbances for sensitive components, such as lasers,^[129,130] and it can be unleashed through cavity-enhanced backscattering.^[131] Therefore, it should not be overlooked in the design of photonic integrated circuits.

The theoretical treatment through CMT results in a differential equation for the power in forward and backward propagating modes.^[58,59,65–67] Assuming small perturbations, e.g., surface-roughness or material defects, the system becomes weakly coupled and may be further approximated by decoupling forward and backward propagating modes, allowing for straight-forward calculation.^[58,59,67] This method was applied to the problem of surface-roughness-induced backscattering by Ladouceur and Poladian.^[128] Although this approach is conceptually similar to the PL model for the estimation of surface-roughness-induced scattering,^[74,78] it does not entail the restrictive approximation of the radiation modes by the free-space modes. Morichetti et al. abstract the bespoke model of backscattering in the slab waveguide by discovering an equivalency with the square of the derivative of the effective refractive index with respect to the waveguide thickness.^[129] They study the qualitative agreement of the model by numerically fitting to values measured via optical frequency domain reflectometry (OFDR).^[132] They obtain higher conformity than through fitting a previously devised model for PhC waveguides that is proportional to the mode's group index.^[54] Subsequently, Melati et al. combine this discovery with a similar model of surface-roughness-induced scattering,^[94] as already discussed in Section 2.1. They utilize the gained generality to apply their model to 3D waveguides and show qualitative agreement with measured backscattering losses on diverse platforms^[129,133–135] by fitting the proportionality coefficients numerically. As was the case with the model of surface-roughness-induced scattering, the derivative with respect to the waveguide width corresponds to the contribution of sidewall-roughness-induced scattering and may be extended with an additive term containing the derivative with respect to the waveguide height to include the top- and bottom-roughness-induced backscattering.

Peng et al. investigated the sources of backscattering for various straight waveguides of different geometries and materials.^[130] They determined the backscattering through OFDR for their fabricated waveguides and polarizations. Subsequently, they analyze dominant backscattering source by mode overlap calculation. They find that the backscattering in their SOI platform can be explained by the overlap with the sidewall, lending evidence to predominating sidewall-roughness-induced backscattering. The backscattering in their SiN platform was traced to the combined effect of the sidewall roughness and defects in the cladding. They explain the difference by the weaker confinement compared to SOI. However, they did not investigate the roughness' spectral characteristics of their technology. Hence, the discrepancy could also be due to this aspect or the combined effect due to shifted spectral bands of the roughness which contribute to backscattering.

Morichetti et al. further investigated the backscattering in RR systems.^[131] Owing to cavity-enhanced backscattering, its contribution is drastically increased near the resonances. They heuristically correlate the backscattering averaged over a wavelength

range of 10 FSR to the square of the group index of the RR and observe good agreement, thereby reproducing the model of backscattering in PhC by Hughes et al.^[54] In fact, backscattering is a major limitation for RRs and needs to be carefully administered.^[136–138]

2.4. Leakage

Substrate leakage is yet another important effect contributing to propagation loss. In principle, it may be made negligible by deposition of a sufficiently thick layer between substrate and waveguide core, which is typically an oxide and called buried oxide (BOX) in SOI waveguides.^[27,31] However, it was shown that for waveguide platforms with weak confinement the substrate leakage may explode and checks against such situations are, therefore, imperative.^[139] In typical design flows, these are conducted through simulations in design suites.^[35] The impact of geometric and material perturbations on leakage may be considered through CMT.^[140]

Rib waveguides, however, feature a special case: lateral leakage. Because the slab section of the waveguide core additionally accommodates a continuum of modes at angles deviating from the waveguide axis, any power coupled to them is transported away from the ridge, and they are therefore also called radiative. Hence, strong coupling and the thereby incurred huge propagation loss may befall the heedlessly designed PIC consisting of rib waveguides. This mishap occurs when the propagation coefficient of the waveguide mode matches the projected propagation coefficients of the slab modes.^[141]

2.5. Discontinuities

Disruption in the longitudinal invariance of the waveguide cause the unperturbed modes of both sides viewed separately to no longer be eigenmodes of the system.^[59] At the junction, a number of modes are excited that may be of higher-order, counter-propagating, and radiative in any of both sides. Hence, a rigorous treatment requires fully numerical methods.^[142–144] However, assuming slight discontinuities and weak perturbation allows semianalytical evaluation exerting exclusively the unperturbed modes in a simple overlap integral.^[145,146]

2.6. Bend Loss

Bent waveguides accommodate modes whose field profile is shifted outwards^[147] and which necessarily become radiative.^[59,148] The radiation in the bends may be computed through conventional simulations with PMLs as boundaries,^[149] the BPM,^[150] FEM,^[151] or through considering radiating dipole sources like in VCM.^[152,153] The loss due to mode-mismatch at the junction between straight (or curved differently) and bent modes may be computed as explained in Section 2.5 or through conformal mapping^[148] in conjunction with CMT.^[154] Another possibility is to use the BPM for a unified treatment of insertion and propagation loss.^[150] Furthermore, the modes' dislocation leads to increased overlap with the outer sidewall. Hence, sidewall-roughness-induced scattering (out-of-plane and backscattering) is increased.^[117]

2.7. Surface Roughness Analysis

Looking at any herein discussed models of surface-roughness-induced scattering and backscattering, it is evident that the characteristics of the roughness is an integral and crucial aspect. In fact, it was established that the spectral properties of the roughness' stochastic process are the determining factor and the importance of surface roughness analysis has been pointed out at several instances.^[98,112,155,156] However, it did not receive the attention its significance would merit. All works that came to the authors' attention and that are mentioned in the following discussion *a priori* treat the autocovariance of the process generating the surface roughness as being writable as a function whose parameters consequently fully describe both the roughness and the resulting scattering. Therefore, the conducted analysis is known as parametric spectral inference in the literature covering stochastic processes. The procedure through which these parameters are determined is of utmost importance. Conversely, a statistically motivated and objective criterion for model selection or parameter optimization with respect to the autocovariance's functional family and the corresponding parameters is lacking in the literature. That is, the postulated autocovariance function were either exponential^[54,75,77,79–81,88,90,94,98,129,157–160] or Gaussian.^[53,119]

Regarding the parameter estimation, the autocovariance was often simply assumed^[76,119,161,162] or it was copied from other studies whose roughness was presumed to be similar, e.g., ref. [157] use values from ref. [163] which determined them in ref. [88] and ref. [31] utilized data from ref. [164]. In other instances, the estimation procedure is unclear^[53,88,156,158] or is not detailed altogether.^[82,89,129] The most thorough spectral inference typically conducted for surface roughness data was based on the controversial variogram regression. That is, the SAC, itself being a nonparametric estimation of the process' autocovariance, is treated as if it were data. Usually, the proposed autocovariance function was fit through least squares regression (LSR)^[165,166] or through an optical fit.^[81,85] Variogram regression also enjoys popularity in other sciences, see e.g.,^[167] From a statistical point of view, however, estimators based on the SAC are inefficient,^[168] and it is generally advised against estimating the autocovariance parameters through using the SAC in lieu of the true autocovariance in estimator expressions,^[169] which is a necessary step through which variogram regression is motivated. The least squares estimator (LSE) acquired through LSR of the SAC, in particular, is not justified. That is, statistical estimators should in general be motivated through maximum likelihood (ML) arguments,^[170] and for LSR to be ML, the data needs to be independent and identically distributed stemming from a Gaussian distribution. While the finite sampling properties of the SAC are extremely complicated, an argument can be made to qualify for the latter requirement in the large sample case through its asymptotically normal quality.^[171] The individual coefficients, however, are usually highly correlated and only independent for an entirely random process.^[172] Therefore, it is evident that the LSE should be expected to have a bias. Thus, it is inconsistent and will not converge towards the true parameters of the underlying process regardless of the number of data points.^[173] Their covariances also exhibit nontrivial dependencies

on the sum of all coefficients of the *true* autocovariance, and, thus, they are not easily computed.^[174] Nevertheless, while certainly ambitious, it is conceivable that the procedure could be extended through generalization of the regression method^[175] and modelling of the covariance structure of the SAC coefficients.^[176] This could also enable estimations of the parameter estimates' variance. However, what usually is left out of the discussion is that these arguments are brought forward for a process with *a priori known* mean and may therefore set zero without loss of generality. Since the mean function is unknown for real data, its estimation again induces a bias in the SAC itself for finite samples^[171,177] and invalidates the asymptotic normality for certain long-memory processes.^[178] Derivative estimates will, therefore, deteriorate. Furthermore, a similar effect can be expected from a trend in the data, such as a tilted AFM stage. Moreover, two definitions for the SAC exist: a biased and an unbiased version. While the biased version is generally preferred due to, *inter alia*, its lower variance,^[171,177] for regression purposes, it is obviously preferable to utilize the unbiased definition. That all being said, in practice, variogram regression appears to just work and little differences were observed for real data^[179] and especially for large sample sizes.^[180] Optically fitting the SAC, however, should be avoided since visually small differences in the SAC can lead to larger gaps in the spectral domain.^[170]

Treacherously, however, the lack of an objective decision criterion holds the danger of falling victim to circular reasoning. In several instances, the roughness was not directly measured from samples fabricated in the corresponding process but was assumed or fit such that the subsequently utilized model satisfyingly reproduces the measured propagation losses. In itself, this is not an issue at all, as it allows to investigate the qualitative behavior of the model and its dependencies on parameters. However, in some subsequent works, those instances were used to argue in favor of the applied models, most often the PL model.^[78] However, these all are subject to the herein discussed approximations and limitations. Similarly, it is certainly worth to investigate whether simple, efficient models may be applied to those systems, whose complexity surpasses the underlying approximations, through further assumptions or abstractions in order to bring estimation and measurement closer. Nevertheless, extreme care must be taken not to evoke a self-fulfilling prophecy. To this end, reliable error estimates of the model used and thorough uncertainty analyses of the underlying measurement data or derivative parameters should be carried out to a greater extent.

Hence, it is evident that the spectral analysis is in dire need of renewed attention. One straight-forward improvement is to transform into the spectral domain and consider the periodogram instead of the SAC. The reason is that the periodogram is distributed like a χ^2_2 -distribution (2 degrees of freedom) with constant variance for the nonzero frequencies and like a χ^2_1 -distribution (1 degree of freedom) for the 0 ordinate.^[172,177] Additionally, the periodogram ordinates are asymptotically uncorrelated.^[177] Hence, statistically consistent regression is plausible in the large sample case.^[180,181] However, when the sample mean is subtracted from the data, the χ^2_1 -distribution ceases to be valid for the 0 frequency ordinate, since it becomes identically 0.^[177] Another option is to directly maximize the

process' likelihood function to obtain the parameter estimates. With the assumption of a Gaussian process, the likelihood function may be directly computed. However, this procedure scales with $\mathcal{O}(n^3)$ complexity.^[182] For typical roughness measurement data it is, thus, unsuitable. Instead, quasi-likelihood methods are usually used for the parameter estimation.^[183] Prominently, the Whittle likelihood has a complexity of $\mathcal{O}(n \log(n))$ and is extendable to higher dimensional and missing data.^[184,185] Finally, hypothesis testing and model selection can be based upon the Whittle likelihood,^[186–188] which promises to usher in objective model selection and parameter estimation that includes uncertainty analysis.

2.8. Case Studies and Design Guidelines

After visiting the individual contributions to the propagation loss and the respective models the question remains: How does the waveguide geometry and the refractive index contrast *generally* impact the propagation loss? This question is most relevant to designers of the PIC, who focus on choosing a certain geometry conformal to the requirements of the selected foundry. And yet, the number of relevant parameters is too high and most of them are too intertwined to give independent and meaningful scaling laws. The only exceptions are the parameters that are usually small and treated as perturbations in the (semi-)analytical models. Regarding surface-roughness-induced scattering, this is the RMS value of the surface roughness whose square linearly scales the contribution to the propagation loss. In Equation 13 this relationship is enclosed in $S_z K_y$, i.e., the roughness' spectral properties. Regarding absorption, the imaginary part of the permittivity of the waveguide materials linearly increases the absorption loss according to Equation 15. On the other hand, the light's frequency ω (or, equivalently, the wavelength) is an important parameter, and prefactors are present both in the expressions for scattering and absorption. However, a second dependency of the electric fields of the mode on ω is somewhat hidden and a combined scaling law is currently not available.

To derive an answer in spite of these issues, we compute the propagation loss of two representative strip waveguide systems in a perturbative treatment. This method relies on the electric fields of the mode computed in a simulation suite, the complex permittivity of the materials used, and the spectral characteristics of the roughness at the material interfaces. The modes are computed in Ansys Lumerical (version: 2022 R2, module: MODE, solver: Finite-Difference Eigenmode (FDE)). The material properties were set with a vanishing imaginary part of the permittivity, such that the loss computed by the FDE solver directly represents radiative losses with the interaction of the PML boundaries. The surface-roughness-induced scattering is computed via the VCM model devised by Hörmann et al.^[114] If an assessment over a range of frequencies is of interest, this procedure may be readily repeated with the appropriate parameters.

2.8.1. Silicon on Insulator (SOI)

First, we examine a SOI waveguide platform for the operation at the standard telecom wavelength of 1550 nm. It consists of a high-density-plasma (HDP) silicon oxide substrate, a silicon strip

waveguide, and a sputtered silicon oxide cladding. The complex refractive indices of the materials are listed in Table 2. Concerning the surface roughness, only the sidewalls were modeled, which is typically the dominating contribution. The exponential kernel and its variance and correlation length in the waveguide axis were adopted from the estimation based on AFM measurements conducted by Horikawa et al.^[85]: 1 nm² and 20 nm. The correlation length in the waveguide height axis was not based on measurements and instead inferred for an exponential kernel to best fit the measured propagation loss, resulting in 220 nm.^[114] The roughness on both sidewalls was assumed to be uncorrelated. The resulting sidewall-roughness-induced scattering and radiation losses of single-mode platforms of either TE or TM polarization are plotted in Figure 4. It is apparent that high and narrow waveguides lead to high scattering. Fixing the waveguide height, the scattering generally decreases with increasing width as the confinement is increased. Contrasting TE and TM polarizations, the well-known fact is reproduced that the TM polarization features reduced scattering. The explanation for these observations can be found in the higher overlap with the sidewalls in these configurations. When comparing these estimations with the BH model,^[75] we obtain overall lower losses. Especially for the TM polarization the maximum value is decreased by a significant amount. The difference in the modeled correlation lengths (50 nm was used in^[75]) partly explains this alteration. Nevertheless, both models agree in a qualitative sense and the general impact of the waveguide geometry is similar. However, the question arises: How certain can the applicant of a certain chosen model be about the estimation? Strictly speaking, prudent error estimation via, e.g., a suitable series expansion of the models under consideration should be conducted to provide a quantitative answer. However, such an analysis is currently not available. Therefore, the underlying assumptions elaborated in Section 2.1 of these models may induce inaccuracies of varying magnitude, and this certainly contributes to the discrepancy observed above. A commonality of the models that do not compute the true radiation modes is that the smaller the waveguides and the higher the refractive index contrast the more errors are incurred.^[98] Hence, future research on the topic of error estimation is encouraged to equip the modeling of surface-roughness-induced scattering with more confidence.

For all but the smallest waveguides, the radiation loss is negligible. Yet, in the cases where the radiation loss is high, a large interaction with the simulation boundaries causes the estimated loss. In these instances, the nonzero fields of the barely guided

Table 2. Complex refractive index of the SOI platform at a wavelength of 1550 nm: the real part of the refractive index n , its imaginary part (the extinction coefficient) k . The refractive indices of the silicon oxides were determined through ellipsometry.^[117] The refractive index of the silicon material was taken from literature.^[216]

Section	Material	n	k
Core	Silicon	3.476	0
Cladding	Sputtered silicon oxide	1.477	1.461×10^{-14}
Substrate	HDP silicon oxide	1.451	1.164×10^{-14}

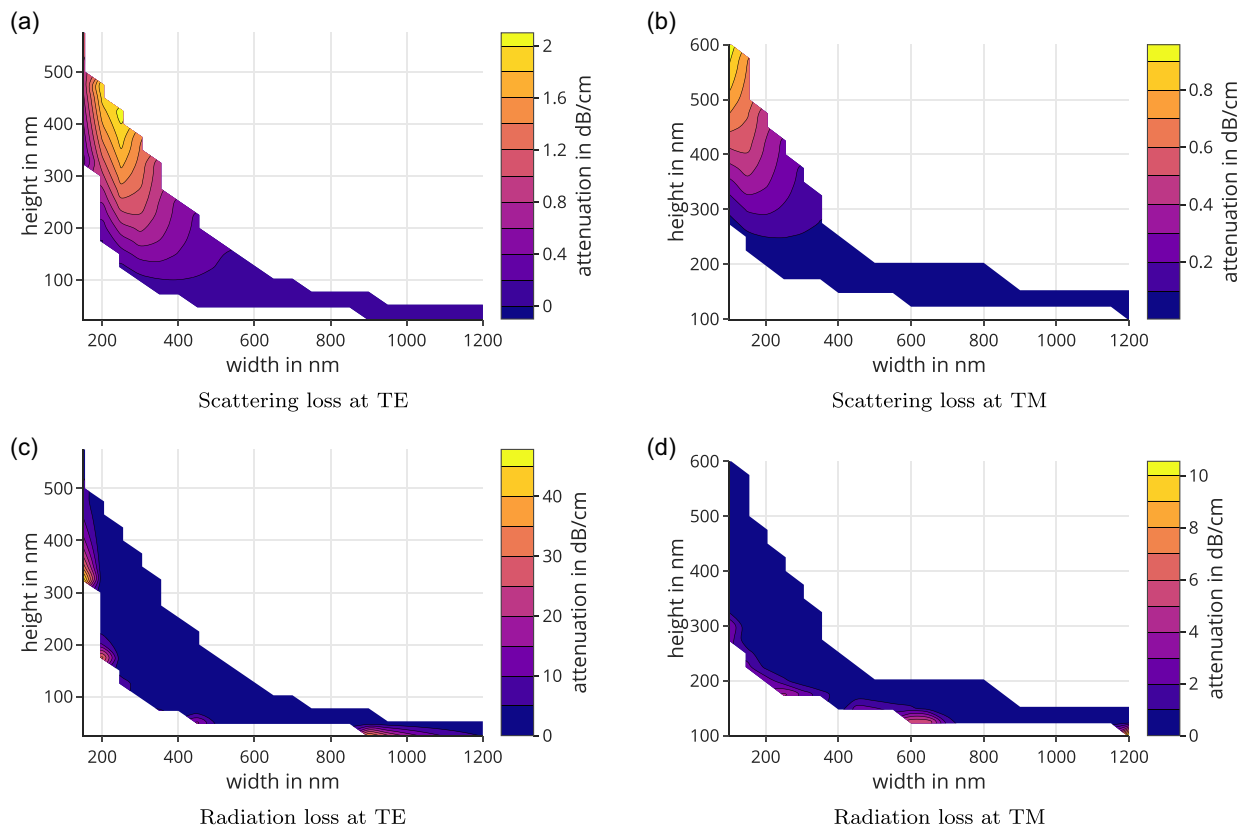


Figure 4. Modeled sidewall-roughness-induced scattering and radiation loss in a SOI single-mode waveguide platform operated at 1550 nm. The scattering in a,b) is determined from the modes' field profiles in a perturbative calculation based on.^[114] The radiation loss in c,d) is taken directly from Lumerical.

modes at large distances can interact with the substrate, other waveguides, or metals in the vicinity, leading to leakage, cross coupling, or absorption. Hence, checks against leakage and other coupling losses are imperative, especially for small platforms. From the extinction coefficient of the materials, it can be deduced that the absorption is negligible for this platform. This is a commonly used assumption for SOI platforms and reproduced in this instance. Attenuation values due to absorption loss (computed in the same manner as in Section 2.8.2) remain in the order of $1 \times 10^{-9} \text{ dB cm}^{-1}$.

2.8.2. Silicon Nitride

Second, a CMOS-foundry-sourced silicon nitride waveguide platform is considered.^[189] Silicon nitride has the advantage that wavelengths down to the visible spectrum are available.^[57] Attractive applications include biosensors, since wavelengths in the therapeutic window may be targeted.^[190,191] Accordingly, we set the wavelength to 850 nm. The cladding and substrate remain sputtered silicon oxide and HDP silicon oxide, respectively. The material parameters of operation were measured via ellipsometry, and the results at the wavelength are tabulated in Table 3. To estimate the scattering loss, all waveguide interfaces were considered. The radiation loss was computed as before. However, absorption loss is non-negligible for this platform because of the relatively large extinction

Table 3. Complex refractive index of the silicon nitride platform at a wavelength of 850 nm: the real part of the refractive index n , its imaginary part (the extinction coefficient) k . The refractive indices of silicon nitride and the silicon oxides were determined through ellipsometry.^[117]

Section	Material	n	k
Core	Silicon nitride	1.989	1.204×10^{-6}
Cladding	Sputtered silicon oxide	1.481	7.609×10^{-13}
Substrate	HDP silicon oxide	1.454	2.257×10^{-13}

coefficient of the silicon nitride core. To account for this contribution, the sensitivity to perturbations of the core is computed in the respective materials and multiplied with the imaginary part of the permittivity, i.e., as in Equation 15. This approach provides a unified perturbative treatment of both surface-roughness-induced scattering and absorption. The spectral properties of the surface roughness were inferred from 2D AFM measurements via spectral analysis based on the Whittle likelihood analogous to ref. [115]. To this end, the roughness' autocovariance was parametrized by a separable, anisotropic autocovariance function featuring an exponential kernel in the transverse axis, and a Matérn ($\nu = 3/2$) kernel in the longitudinal axis. The resulting spectral parameters are tabulated in Table 4. They

Table 4. Spectral parameters of the roughness of the waveguide's surfaces inferred from atomic force microscopy^[17] based on maximizing the Whittle likelihood.^[15] ν is the variance, and l_1, l_2 are the transverse and longitudinal correlation lengths, respectively.

Surface	ν in nm ²	l_1 in nm	l_2 nm
Sidewall	12	2600	170
Top	0.1	1	7
Bottom	0.1	1	7

indicate that the sidewall-roughness-induced scattering is dominating because of its exceeding magnitude. The estimations of the contributions to the scattering loss are depicted in **Figure 5**. Overall, the surface-roughness-induced scattering dominates, except again for the weakly guided platforms with small geometries and high radiation loss. Qualitatively, the maximum of the scattering loss occurs again at high and narrow waveguides whose modes have a high overlap with the sidewalls. However, for applications that depend critically on the propagation loss values, absorption can no longer be neglected. What is more, the

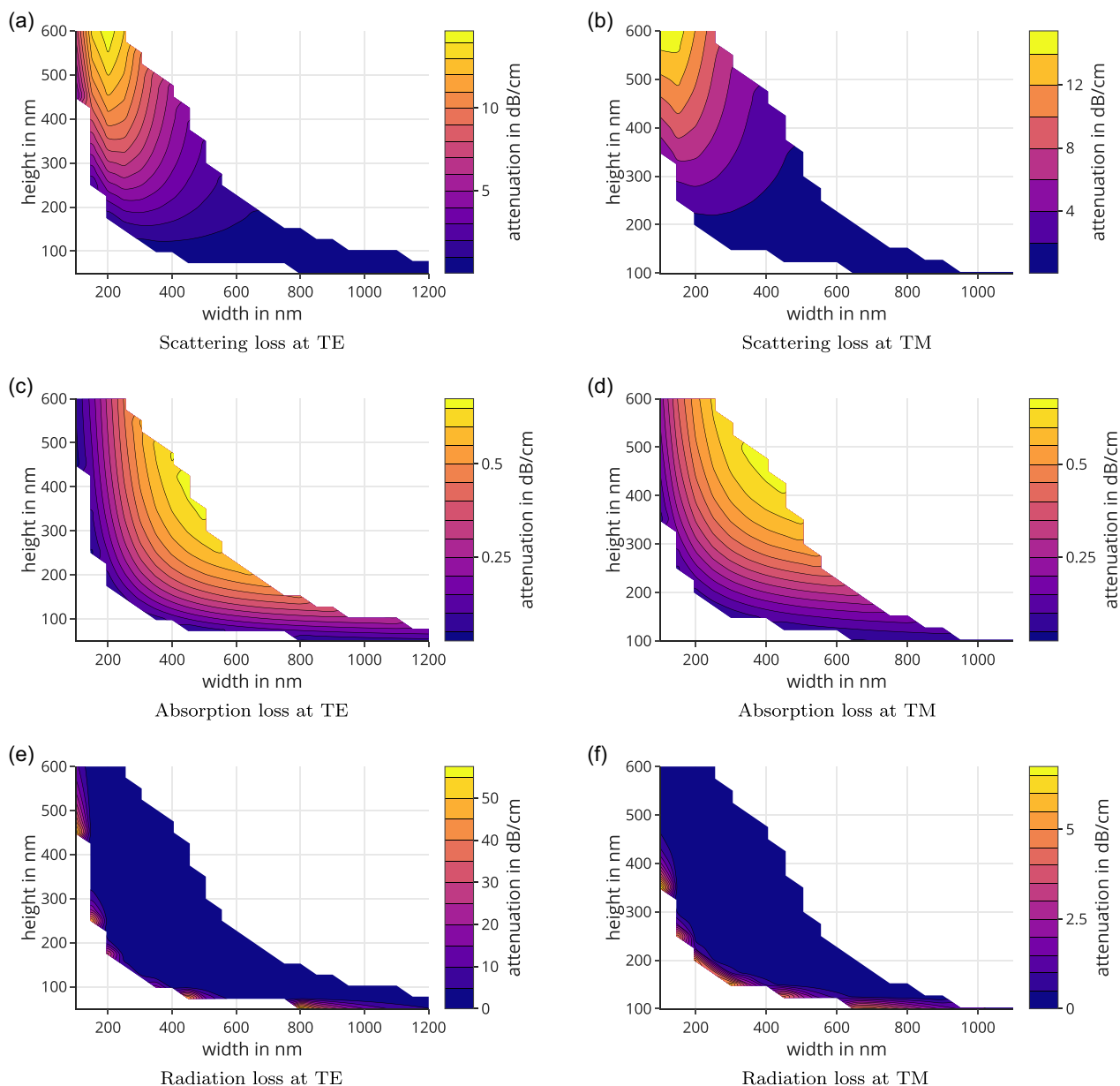


Figure 5. Modeled contributions to the propagation loss in a silicon nitride, single-mode platform operated at 850 nm. a,b) The scattering in a) and b) and c,d) the absorption in c) and d) are determined from the modes' field profiles and the underlying ellipsometry and AFM measurements in a perturbative calculation. e,f) The radiation loss in e) and f) is taken directly from Lumerical. (a,c,e) The left column depicts the estimations for the TE mode and (b,d,f) the right column the ones for the TM mode.

contribution of the absorption does not vanish as fast as the scattering's for wide waveguides, leading to a convergence of the total propagation loss w.r.t. the width. Including the absorption for the purpose of explaining, this effect was previously found to be necessary to achieve quantitative agreement with measured propagation loss.^[117] When considering this compound effect in comparison to the application of the PL model on a similar platform^[192] and the good quantitative agreement in both instances, this indicates that further care should be taken to carefully dissect and distinguish the individual contributions to the propagation loss. Depending on the material platform and the specific foundry at hand, the magnitudes of surface-roughness-induced scattering and the absorption may vary.

2.8.3. Design Guidelines

Reflecting on the above case studies, we derive general design guidelines for the PIC designer to achieve low propagation loss in their waveguides. 1) Increase overall waveguide size and, if possible, width. By increasing the size of the waveguide, mode confinement can be increased and overlap with sidewall roughness can be avoided. Sidewalls typically are the main contributor to the surface-roughness-induced scattering in strip waveguide systems and to the total propagation loss. More complex surface roughness may occur for different waveguide geometries, such as rib waveguides, and more involved approaches may be called for. Too wide waveguides may incur increased bend losses,^[117] creating the need for larger bend radii or, e.g., Euler bends.^[193] If single-mode operation is a requirement, the waveguide cannot be made wide enough at large heights to achieve low scattering, indicating a benefit of lower and wider waveguides. On the other hand, larger multimode waveguides feature higher confinement and lower scattering. Simultaneously, they can be engineered to feature low-crosstalk with only a moderate increase in footprint, even considering bends.^[194] 2) Use TM polarization. Modes of TM polarization avoid electric field side-lobes located near/at the sidewalls, further decreasing overlap with these rough surfaces. Consider that for typical waveguide geometries with larger width than height which feature a mode of TM polarization usually also allow one or more modes of TE polarization. This potentially requires additional polarization management. 3) Check against absorption. Checking the contribution of the absorption is important, especially if a waveguide geometry with low scattering was achieved. 4) Check against leakage. Too low confinement may lead to substrate leakage, cross coupling to nearby waveguides, or absorption at metal structures.

2.8.4. Material Platforms

In this section, we considered as case studies the waveguides made in SOI and SiN. waveguides made using III–V semiconductors are well established and their propagation loss, which is typically high, can be reduced to 0.45 dB cm^{-1} .^[195] Beyond SOI, SiN and III–V, several emerging platforms merit attention: chalcogenide rib guides already achieve 0.3 to 0.5 dB cm^{-1} loss in the 2 to $5 \text{ }\mu\text{m}$ band;^[196,197] hot-embossed polymer waveguides report 0.1 dB cm^{-1} at 850 nm ;^[198] graphene or graphene-oxide overlays add active and nonlinear functionality with absorption

coefficients of $\approx 0.2 \text{ dB }\mu\text{m}^{-1}$ on silicon cores;^[199,200] plasmonic silver stripes can confine light below the diffraction limit while keeping losses below 1 dB cm^{-1} ;^[201] and thin-film LNOI now combines 0.37 dB cm^{-1} propagation with large Pockels modulation efficiency.^[202]

3. Experimental Section

Experimental techniques for estimating the propagation loss in microphotonic waveguides encompass a wide range of methods, each with its unique advantages and critical aspects. The methodologies range from straightforward approaches to advanced techniques. They include the most accurate reflectometry-based methods, commonly used standard methods such as the cut-back technique, scattered light measurement, and the Fabry–Perot resonance method, as well as more sophisticated methods that rely on ring resonators or interferometer-based setups. The methods described here are intended mainly for single-mode waveguides, but some of them can be adapted to multimode waveguides exiting a specific mode using prism couplers.^[203]

Reflectometry, particularly OFDR,^[204] is well-known for its precision in characterizing waveguides. OFDR provides an accurate view of the waveguide by analyzing the backscattered light, revealing details such as propagation loss, scattering centers, group delay, and chromatic dispersion with remarkable accuracy. This method stands out for its comprehensive results, though it demands sophisticated instrumentation and an in-depth understanding of optical phenomena. Optical reflectometry allows for the measurement of the intensity of the optical power that is reflected back from a specific propagation distance, d_0 , within a waveguide. Given a waveguide that is uniform and does not change in the direction of propagation, the power backscattered from the waveguide cross section at the propagation distance d_0 is directly proportional to the propagating optical power at d_0 . By measuring the amplitude of the return loss, the propagation loss can be computed. In fact, the waveguide's propagation loss can be determined by dividing the slope of the return loss dependence on the distance in half.

OFDR utilizes the Fourier transform to derive time domain return loss statistics from frequency domain data. The spatial domain is thereafter determined by the group index of the propagating mode. This technique has been employed to analyze an extremely low loss strip waveguide in Si_3N_4 technology with width = $2.8 \text{ }\mu\text{m}$ and thickness in the range from 80 to 100 nm .^[27] Figure 6 illustrates the measurement of the reflectometry for a 6-meter-long spiraling waveguide. The inset displays a linear regression analysis applied to the diminishing return loss amplitude data, which is utilized to determine the propagation loss, which ranges from 3 to 5 dB m^{-1} depending on the thickness value. The estimated uncertainty in this measurement is a mere 0.01 dB m^{-1} .

The method relying on arrayed waveguide gratings (AWGs) represents a niche yet insightful approach,^[82] based on the differential loss analysis of arrayed waveguide structures. It distinguishes itself by its independence from coupling efficiencies, focusing on the loss characteristics intrinsic to the waveguide paths themselves. The main drawback of this approach is related to the relatively large footprint of the AWG-based test structure,

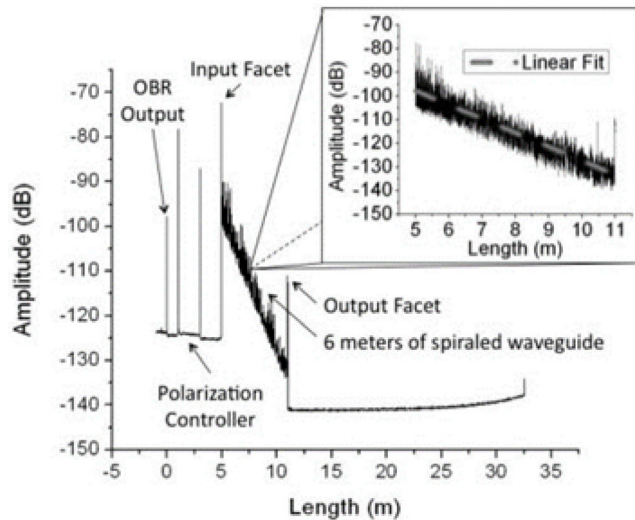


Figure 6. OFDR technique applied to optical characterization of 6 meters of spiraled waveguide in Si_3N_4 technology. The inset shows how propagation loss is extracted by linear fitting the decreasing return loss amplitude. Reproduced with permission.^[27] Copyright 2011, Optical Society of America.

which is of the order of 1 cm^2 for standard silicon waveguides, and the complexity of the measurement setup.

With the above-mentioned methodologies outlined, we delve into the specifics of standard approaches and those considered as advanced harnessing the potential of ring resonators and interferometers, illustrating the techniques at our disposal for probing the waveguide propagation loss.

3.1. Standard Methods

The cut-back method^[205] relies on comparing the transmission through progressively shorter waveguide lengths, offering a straightforward measure of propagation loss. Ultimately, the length dependency is fit to obtain the loss coefficient. Its simplicity belies the meticulous attention required to ensure consistent coupling conditions, which presents a significant challenge for experimental setups in the real-world and the method's main shortcoming. Specifically, the steps for implementing the cut-back method are as follows: 1) the transmission T , which is the ratio of the output power P_{out} to the input power P_{in} , is measured for each waveguide of length L ; 2) the experimental data is displayed in a T vs. L format (see **Figure 7**); and 3) the propagation loss is determined by calculating the slope of the best linear fit of the experimental data.

The most challenging aspect of this methodology is to precisely and consistently measure the transmission T . A widely used approach involves quantifying the power at the detector and subsequently dividing it by the power output by the laser diode. Nevertheless, the process of connecting a cleaved facet with a lensed fiber is highly sensitive and prone to variation between different waveguides. Moreover, fluctuations in temperature or other external variables could impact the total transmission.

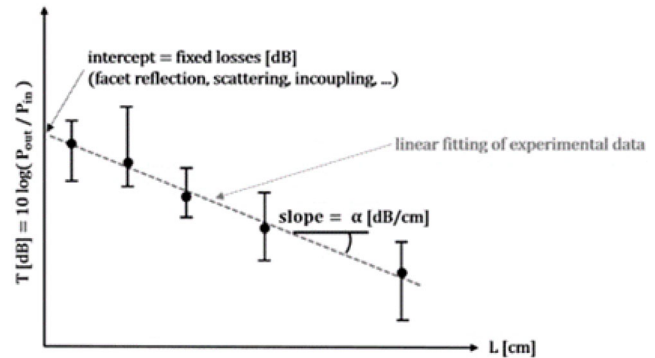


Figure 7. Typical T vs. L plot. The propagation loss is extracted from the slope of the linear fit of experimental data.

For measuring the propagation loss of waveguides down to the order of 1 dB m^{-1} , several spiral waveguides of different length are required. As an example, **Figure 8** displays two chips that have been manufactured specifically for the purpose of evaluating the propagation loss of a conventional strip silicon waveguide.^[206] The footprint is $\approx 0.3\text{ mm}^2$ for both the chips.

The cut-back method can be considered as a basic technique for detecting propagation loss values that are on the scale of a few dB cm^{-1} . However, achieving satisfying accuracy necessitates the use of multiple lengthy spirals, which occupy a significant amount of space, roughly 0.5 mm^2 for standard silicon waveguides. Furthermore, in order to precisely quantify very low propagation loss values, the waveguides' lengths should be extended even further to distinguish the slight disparities in their transmissions. Consequently, this approach becomes unfeasible for measuring waveguides with ultralow propagation losses.

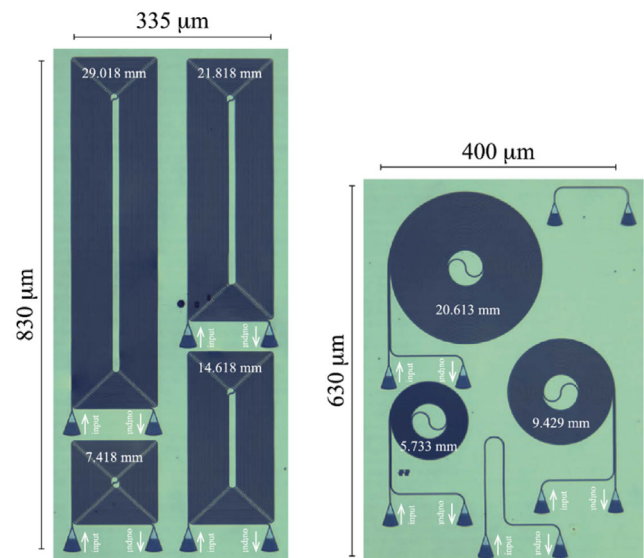


Figure 8. Examples of silicon photonics chips for measuring on-chip waveguide loss by the cut-back method: (left) rectangular spirals; (right) Archimedean spirals. Reproduced with permission.^[206] Copyright 2020, Optical Society of America.

In scattered light measurement,^[207] the measure refers to light that escapes the waveguide normal to the chip and can be detected by a scanning fiber or through imaging on a detector array. Particularly effective for higher-loss materials and guiding structures, its utility fades as waveguide quality improves, reflecting its role in the initial stages of waveguide development. Optical fibers have the capability to gather dispersed light from the surface of a waveguide and can be moved across the surface in a scanning motion. Alternatively, one can create a complete image of the entire surface and then determine the decay of dispersed light correspondingly. The scattering of light is measurable only when there is a high level of loss in the waveguide and a relatively high power is being transmitted through it. In numerous scenarios, neither option is preferable, and as a result, this approach is typically employed for preliminary investigations of waveguides, particularly when there are significant losses. However, it is abandoned in favor of alternative ways after the waveguide has been optimized.

The Fabry–Perot resonance method,^[208] treating the waveguide as a resonant cavity, leverages the interference patterns created by light reflections within the waveguide. It offers a multifaceted view, sensitive to both the material and geometric aspects of the waveguide, enriching our understanding of waveguide behavior. An optical waveguide with polished or etched endfaces bears a resemblance in structure to the cavity of a laser. Light travels through the waveguide and can bounce off either end, depending on the refractive index of the waveguide material and the surrounding medium (usually air). As a result, the waveguide can be seen as a resonant cavity, where the waves reflect multiple times as they move along the waveguide and return. A cavity of this nature is referred to as a Fabry–Perot cavity.

The propagation loss, measured in cm^{-1} or m^{-1} , can be calculated using the following formula

$$\alpha = -L^{-1} \ln \left(R^{-1} \frac{\rho^{1/2} - 1}{\rho^{1/2} + 1} \right) \quad (16)$$

R represents the reflectivity of the facet, L is the length of the waveguide (measured in centimeters or meters), and ρ represents the ratio of the highest intensity to the minimum intensity in the spectral response of the Fabry–Perot cavity. **Figure 9** shows the calculated spectral response for a Fabry–Perot cavity with $R = 0.31$, the typical value for silicon waveguides, $L = 1 \text{ cm}$, and propagation loss $= 1 \text{ dB cm}^{-1}$. In the experiments, the propagation loss can be easily measured by estimating ρ for the spectral response and R by calculations. However, obtaining an accurate value for R can be challenging, as the facets may be tilted by an unknown amount or exhibit spurious roughness. These imperfections can lead to significant deviations between the calculated and actual values of R , potentially resulting in an overly optimistic estimation of the waveguide loss.

A Fabry–Perot experimental investigation can provide supplementary information. If the waveguide is multimode, the presence of additional interference results in distortion of the response. This distortion provides information on the waveguide's mode characteristics, indicating whether it is single-mode, slightly multimode, or highly multimode.

In order to obtain precise measurements of waveguide propagation loss using the Fabry–Perot method, it is important to have

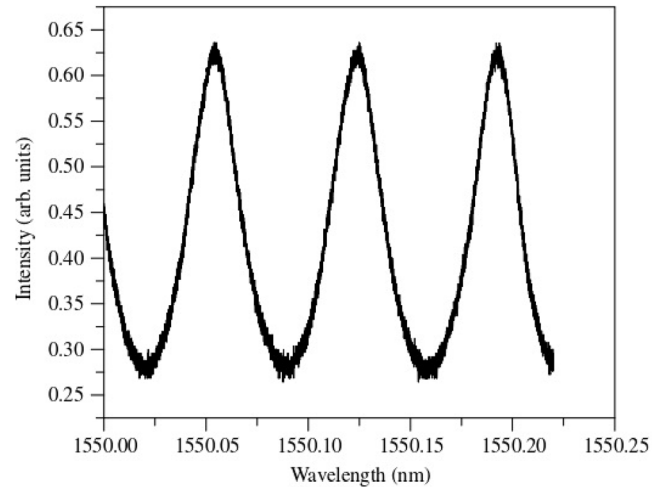


Figure 9. Spectral response of a Fabry–Perot cavity formed by a typical single-mode silicon waveguide.

a significant difference in fringe intensity to minimize uncertainty. Additionally, the round-trip loss of the waveguide should be similar to or greater than the loss caused by reflection at the end of the waveguide.

3.2. Advanced Experimental Approaches

As already mentioned, techniques that leverage the principles of ring resonators and interferometry have emerged as promising advanced tools in accurate characterization of propagation loss. The principle that guides all the methods based on ring resonators is the identification of specific ranges of bending radii where the impact of bending loss is minimized, if not entirely negated. For all waveguides, there exists a radius value such that for radius values larger than that cut-off values the bending loss is negligible. This characteristic is particularly pronounced in waveguides with high index-contrasts, such as those fabricated from silicon strips, where resonators with a radius exceeding a few μm or a few tens of μm exhibit negligible bending loss. The initial endeavors to quantify propagation loss through ring resonators introduced a formula that, while not universally applicable, laid the groundwork for further methodological advancements. These subsequent developments have embraced a more comprehensive approach, often incorporating multiple resonators to refine the accuracy of propagation loss measurements.

This first formula^[209,210] is intended for a resonator coupled to just one bus waveguide and relates the propagation loss in cm^{-1} or m^{-1} to the ring resonator finesse F , the ring radius R , and the minimum T_m in the normalized spectral response of the resonant cavity

$$\alpha = [FR(1 + \gamma)]^{-1} \quad (17)$$

where the parameter γ is given by the smaller of the two solutions for γ in the following equation

$$\gamma = \frac{1 \pm T_m^{1/2}}{1 \mp T_m^{1/2}} \quad (18)$$

An alternative approach again based on ring resonators exploits the Q-factor, a metric that quantifies the energy retention capability of the resonator, influenced by cavity loss including those due to external coupling. The Q-factor of an optical resonator is limited by loss, part of which can result from coupling to the external world, i.e., bus waveguide(s). The intrinsic Q-factor Q_{int} is the value which results without considering the mentioned coupling; this is higher than the loaded Q-factor obtained accounting also the coupling. The optical characterization of ring resonators allows for the measurement of only the loaded Q-factor. The propagation loss of the waveguide, assuming negligible bending loss, is related to Q_{int} according to the formula

$$\alpha = \frac{2\pi n_g}{\lambda Q_{\text{int}}} \quad (19)$$

where n_g is the group index of the propagating mode, which can be accurately estimated from numerical simulations only if the waveguide cross section is well-characterized, and λ is the resonator's operating wavelength. If the ring resonator is weakly coupled to the bus waveguide(s), Q_{int} is very close to the loaded Q-factor, the only measurable quantity. In this condition, the propagation loss can be extracted by the experimental measurement of the loaded Q-factor. From a practical point of view, a few ring resonators with different gap values and consequently different coupling strength can be manufactured on the same chip. The ring with the weakest coupling can be selected for the propagation loss estimation, if the Q-factor of that ring can be measured with a good accuracy.^[211] In the given arrangement depicted in **Figure 10**, the leftmost ring exhibits the least amount of coupling, resulting in the lowest transmission at the drop-port and the lowest loss at the through-port when the resonance occurs. Subsequent rings have ever stronger coupling. If the leftmost ring displays a signal level of sufficient magnitude in the drop port to accurately detect a resonance, it can be utilized for

the purpose of measuring loss. If the signal strength in the drop port is insufficient to resolve a resonance, the propagation loss will be approximated using the second ring from the left.

This approach offers a reliable and cautious assessment of the propagation loss. However, it necessitates the manufacturing of several resonators with distinct coupling circumstances and bus-ring gap values. Several techniques utilizing a single ring resonator can be found in the literature. A loss-extraction model based on linear regression was presented and experimentally proven in ref. [212]. This model can be applied to all-pass rings as well as symmetrically and asymmetrically coupled add-drop rings. This model was developed by converting the transmission spectra of a ring into linear relationships, allowing for a linear regression analysis to improve the accuracy of loss measurement. The method was used to estimate the propagation loss of a strip waveguide. The achieved measurement uncertainty exceeds 30%.

Recently, a methodology based on a single ring resonator with a tunable bus/ring coupler was conceived and experimentally studied.^[206] This approach allows for the differentiation between waveguide propagation loss and coupling effects by adjusting the power coupling to the microring and assessing its through-port transmission at varying coupling conditions. This technique is beneficial as it is not sensitive to fiber-chip coupling/alignment errors and does not necessitate expensive equipment for phase response measurements. The algorithm for estimating the propagation loss involves using a tunable coupler within the microring resonator, which is an MZI with a two-point coupling scheme. The coupling is tuned by modifying the phase of the light with a heater above one of the MZI arms, thus varying the output power from the coupler to the ring. By measuring the microring's through-port transmission spectrum at different heater powers, the coupling and propagation losses can be distinguished and quantified. Experimental validation of this method was conducted by fabricating microring resonators with a thermally tunable coupler (see **Figure 11**). The waveguide is a

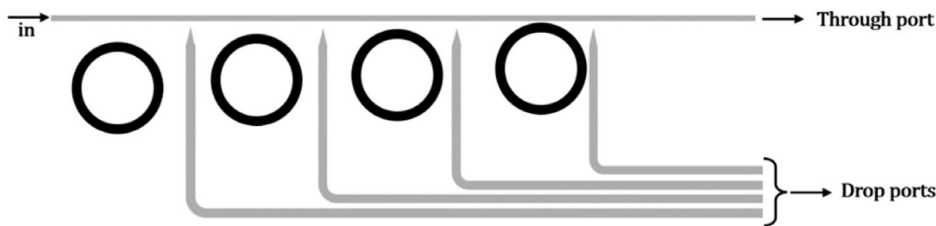


Figure 10. Example of a test structure for measuring the propagation loss using several ring resonators with different coupling conditions with the bus waveguides.

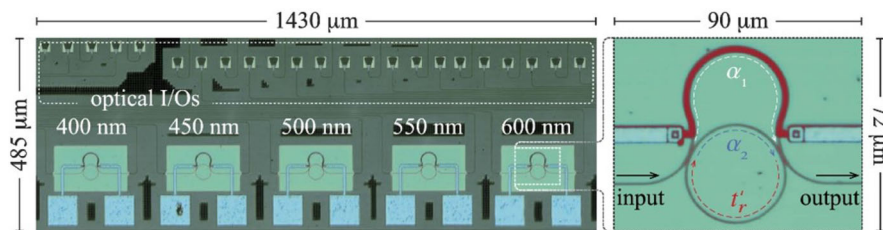


Figure 11. Silicon photonics coupling-tunable microring resonators. The waveguide width varies from 400 to 600 nm in steps of 50 nm. The inset shows a zoomed-in view of a single resonator. Reproduced with permission.^[206] Copyright 2020, Optical Society of America.

silicon strip having core widths ranging from 400 nm to 600 nm. The optical resonance spectra were measured under various heater biases and consequently with various coupling conditions. The propagation losses were then extracted using the developed algorithm, demonstrating the effectiveness of this approach in accurately determining waveguide losses. In particular, the archived measurement uncertainty is at least one order of magnitude less than the measured propagation loss ranging from 3.1 to 1.3 dB cm⁻¹, depending on the waveguide width.

Complementing the ring resonator methodologies, interferometer-based approaches, particularly those utilizing Mach–Zehnder interferometers (MZIs), offer a distinct approach for the characterization of waveguide losses. A very interesting method uses an unbalanced MZI formed by two 2 × 2 couplers connected to each other by two waveguide arms with different path lengths (see **Figure 12**).^[213]

The first step in propagation loss estimation is the experimental measure of the spectral dependence of the optical power at port 3 and 4 when light is launched in port 1 and 2: R_{13} , R_{14} , R_{23} , R_{24} (all dependent on the wavelength). For each of these spectral responses, the extinction ratios are estimated, e.g., $R_{13} = P_{13}^{\max}/P_{13}^{\min}$. The authors derived a quite simple equation relating the propagation loss α to the ratios R_{13} , R_{14} , R_{23} , and R_{24} . The method was applied to the experimental estimation of the propagation loss of a Si₃N₄ strip waveguide. The measured wavelength dependence of R_{13} , R_{14} , R_{23} , and R_{24} is shown in **Figure 13**. Using those spectra, the ratios were computed and the propagation loss was estimated to be equal to 0.25 dB cm⁻¹. The authors verified that the propagation loss measured with their method is very close to the one measured using OFDR (mismatch = 2%), thereby validating the MZI-based method's utility in the accurate measurement of waveguide propagation loss. Finally, we note that uncertainty in some of the above-mentioned methods for propagation loss estimation is ultimately limited by a few well-documented error sources. Bauters et al. demonstrated that OFDR exhibits an uncertainty of 0.4 dB m⁻¹ in estimating the propagation loss in ultralow-loss Si₃N₄ spirals.^[27] For conventional cut-back, the dominant error term is the coupling repeatability; Vlasov et al. quantified facet-to-facet fluctuations that propagate to an uncertainty of ≈10 dB m⁻¹ in high-index-contrast Si-on-insulator waveguides.^[214] Resonant methods inherently average over many round trips; Feuchter et al. reported that, for a Fabry–Perot cavity

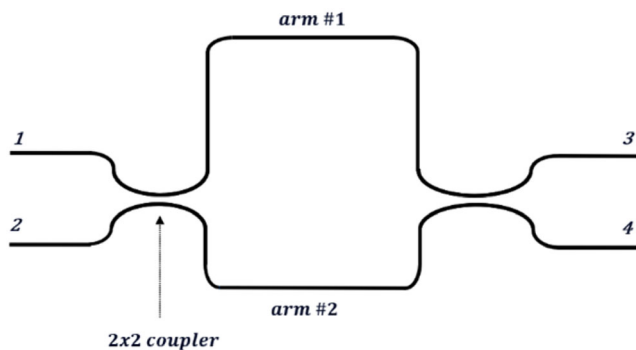


Figure 12. Unbalanced MZI for measuring propagation loss. Reproduced with permission.^[213] Copyright 2016, IEEE.

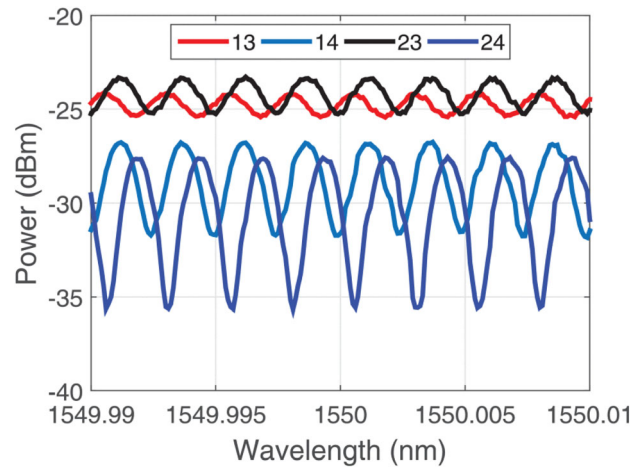


Figure 13. Wavelength-dependent power measured at the four ports of the unbalanced MZI. Reproduced with permission.^[213] Copyright 2016, IEEE.

with high-quality end-facets, the residual uncertainty is an order of magnitude lower (1 dB m⁻¹,^[215]).

4. Conclusion

The accurate estimation of propagation loss in microphotonic waveguides has been significantly advanced by numerical methods. These methods offer remarkable accuracy, with relative errors compared to measured propagation loss often below 5%. This level of precision is particularly beneficial for optimizing the performance of PICs. Furthermore, the numerical approaches allow to model and dissect the different contributions to propagation loss: surface-roughness-induced scattering (both out-of-lane scattering and backscattering), material absorption, leakage. For waveguiding elements such as bends and discontinuities, radiation and coupling loss must be taken into consideration. However, the mentioned numerical techniques require highly detailed and precise physical measurements, such as surface roughness profiles, to ensure accuracy. To that end, it must be taken care to infer only from measurements of the actual waveguide platform one is interested in. Characteristics of seemingly similar fabrication processes might carry over only in a limited manner. Furthermore, the inability to account for small variations in waveguide characteristics may still introduce discrepancies between predicted and actual losses.

While in any particular waveguide platform the importance of the individual contributions to the propagation loss may shift, the surface-roughness-induced scattering was identified as the dominant loss mechanism in a large majority of studies. Unfortunately, it is also the most complex one, largely because of the difficulty of handling the radiation modes. As such, multiple approaches and individual models are available and choosing is a matter of striking a balance between accuracy, time and effort, and simplicity. The investigated models are summarized in Table 1. The goal of the (semi-)analytical models is to provide expressions that solely contain the modes of the unperturbed, i.e., perfectly smooth, system. The strength of the perturbation is a delicate manner because of the discontinuities of the electric

fields at the interfaces and using a well-defined expression should be emphasized, as proposed by Johnson et al.^[62] Such a perturbation is often utilized in mode solvers to speed up conversion. Subsequently, models relying on modes from these suites are also continuous.

The simplest models of surface-roughness-induced scattering rely on perturbation theory and the VCM and heavily simplify both guided and radiation modes by assuming a slab waveguide geometry to give explicit expressions. The most prominent one was devised by Payne and Lacey.^[78] Semianalytical models take the guided modal fields in 3D waveguides into consideration. They further approximate the radiation modes to varying degrees. Barwicz and Haus improve the treatment of the radiation modes of a slab waveguide and propose to extend their model to 3D waveguides by means of the effective refractive index method.^[75] Poulton et al. apply CMT to numerically compute both guided and radiation modes in 3D waveguides accurately.^[98] Ciminelli et al. rely on VCM to approximate the radiation modes while including the guided mode's field profile.^[112] They extend it to incorporate radiation through 3D FE simulations and achieve highly precise estimations.^[79] Hörmann et al. include the 2D characteristics of the surface roughness for the first time in a VCM approach.^[114] These studies on (semi-)analytical models do not provide expressions to compute error estimation. Therefore, a measure of the accuracy of these model is not obtainable, aside from case-wise comparison with measured propagation loss. Hence, the accuracy of the models from Table 1 cannot be generally stated. However, the field would greatly benefit from quantified assessments that enable the comparison of the individual models. Further, it would be important to trace the uncertainties in the estimation back to the uncertainties of the parameters, especially in instances where the measured propagation loss deviates in order to adapt the modeling.

Fully numerical models completely resolve the partly sub-nanometer scale of the surface roughness and evaluate the scattering directly from the simulation. Jaberansary et al.^[53] and Zhang et al.^[119] model the 2D characteristics of the surface roughness and evaluate the scattered power through 3D FDTD simulations, which provide good agreement with measured values. Kita et al. similarly simulate advanced waveguide geometries with low confinement intended for sensing applications to determine whether they provide an advantage, considering the increased propagation losses they incur.^[120]

Material absorption may be an important contributor to the propagation loss and such cases should be screened against. For weakly absorbing material, the corresponding loss may be evaluated through a simple overlap integral Equation 15. If metals or other materials with a high imaginary value in permittivity are present in the waveguide platform with a non-negligible overlap in the electric field, the loss estimation must be conducted within the mode simulation.

Simple scaling laws are not easily obtained owing to the high dimensionality of the parameter space and the inability to factor out subspaces. The exception are the perturbation parameters in the respective models. Regarding surface-roughness-induced scattering that is the RMS of the surface roughness profile whose square (the variance) linearly scales the scattering. For absorption that is the imaginary permittivity of the materials. Another

important parameter is the wavelength which is present in the models for both scattering and absorption in a prefactor. However, a second dependency through the electric field profile is not explicitly apparent. Combined scaling laws considering both impacts are not available but could conceivably be obtained through perturbation theory. Further, the (spatially) spectral characteristics of the surface roughness carry yet more impactful parameters in the form of the correlation length(s) and the functional form of the autocovariance. Up to recently, it was usually assumed that the sidewall roughness are perfect vertical striations and that the remaining autocovariance in the waveguide's propagation axis is of exponential form. It was explained in Section 2.7 that there is evidence suggesting that this is not always the case. Moreover, a robust, statistically motivated procedure to determine the 2D spectral characteristics, including the functional family and its parameters, based on measurements is currently not available. Further, the first model considering the surface roughness as 2D^[114] within VCM brought to light that even slight deviations from perfect striations significantly impacts the scattering loss. In fact, lowering the correlation length along the waveguide height axis reduces the incurred scattering. By contrast, there is a critical value for the correlation length in the waveguide axis that results in maximum scattering.^[90,114]

Two case studies are conducted in Section 2.8 with the goal of finding behaviors common to these widely used material platforms. The methodology relies on a perturbative approach for all of the loss contributions and uses the VCM model by Hörmann et al. for the surface-roughness-induced scattering.^[114] First, a SOI platform operated at 1550 nm, and, second, a silicon nitride platform operated at 850 nm are analyzed. Based on these discussions design guidelines are formulated in Section 2.8.3.

Experimental methods, such as the cut-back method, interferometric approaches, and OFDR, while less complex and faster to implement, offer limited insight into the physical origins of propagation loss. These methods are primarily focused on providing direct measurements of loss without delving into the specific contributions from different sources, such as scattering or material absorption. However, for practical applications, especially when rapid prototyping and testing of waveguides are required, experimental methods remain indispensable. They allow for the quick estimation of losses in fabricated waveguides and for the eventual qualification in a foundry setting. Thus, they enable engineers to evaluate waveguide performance in real-world conditions. **Table 5** summarizes typical propagation-loss requirements by application—telecom, biosensing, quantum photonics, and interferometric gyroscopes—and recommends the simplest loss-estimation technique that attains the necessary resolution (cut-back for $\approx 1 \text{ dB cm}^{-1}$, resonant for $\approx 0.1 \text{ dB cm}^{-1}$ and OFDR for $\leq 1 \text{ dB m}^{-1}$). The combination of numerical and experimental methodologies provides a balanced approach, enabling both detailed understanding and practical measurement, which is essential for the ongoing advancement of photonic integrated circuits. Future developments in this field should focus on further improving the integration of numerical precision and experimental efficiency to optimize waveguide performance and reduce propagation losses.

Table 5. Propagation-loss specifications and recommended characterization strategies for four key application areas. Values refer to continuous-wave operation at 1.3 to 1.55 μm unless otherwise noted; quoted targets are typical figures reported in the cited literature.

Application domain	Typical propagation loss target	Representative mature/emerging platform	Loss estimation technique that reaches the required resolution	Illustrative references
Telecom/Datacom links	$\approx 1 \text{ dB cm}^{-1}$ (0.3 dB cm^{-1} desirable for $<10 \text{ km}$ on-board links)	Shallow-ridge SOI strip waveguides	Two- or three-length cut-back structures; facet-limited repeatability of $\pm 0.2 \text{ dB}$ is acceptable at this loss level	Dong et al. ^[217] , Vlasov and McNab ^[214]
Biosensing (label-free refractometric)	0.05 to 0.10 dB cm^{-1}	Si_3N_4 TriPLeX, low-temperature PECVD or LPCVD cores	Ring/Fabry–Perot resonance analysis or short-range OFDR; thermal stabilisation $\pm 20 \text{ mK}$ recommended	Roeloffzen et al. ^[218] , Deng et al. ^[212]
Quantum photonic circuits (single-photon delay lines)	1 dB m^{-1}	Ultralow-loss Si_3N_4	Optical-frequency-domain reflectometry (OFDR) with 0.01 dB/m precision; cross validation with cavity Q-analysis desirable	Bauters et al. ^[28] , Chanana et al. ^[219]
Interferometric optical gyroscopes (navigation-grade)	$\leq 1 \text{ dB m}^{-1}$ over $\geq 5 \text{ m}$ coil	Si_3N_4 spiral coils with 40 nm core size	Long-range OFDR mandatory	Gundavarapu et al. ^[220]

Acknowledgements

Open access publishing facilitated by Politecnico di Bari, as part of the Wiley - CRUI-CARE agreement.

Conflict of Interest

The authors declare no conflict of interest.

Keywords

microphotonics, numerical methods, propagation loss, silicon photonics, waveguide

Received: April 12, 2025

Revised: August 4, 2025

Published online:

- [1] S. E. Miller, *Bell Syst. Tech. J.* **1969**, 48, 2059.
- [2] E. A. J. Marcetili, *Bell Syst. Tech. J.* **1969**, 48, 2071.
- [3] T. L. Koch, U. Koren, *AT&T Tech. J.* **1992**, 71, 63.
- [4] R. Nagarajan, C. Joyner, R. Schneider, J. Bostak, T. Butrie, A. Dentai, V. Dominic, P. Evans, M. Kato, M. Kauffman, D. Lambert, S. Mathis, A. Mathur, R. Miles, M. Mitchell, M. Missey, S. Murthy, A. Nilsson, F. Peters, S. Pennypacker, J. Pleumeekers, R. Salvatore, R. Schlenker, R. Taylor, H.-S. Tsai, M. Van Leeuwen, J. Webjorn, M. Ziari, D. Perkins, J. Singh, et al., *IEEE J. Select. Top. Quant. Electron.* **2005**, 11, 50.
- [5] R. Helkey, A. A. M. Saleh, J. Buckwalter, J. E. Bowers, *IEEE J. Select. Top. Quant. Electron.* **2019**, 25, 1.
- [6] Y. Kawamura, K. Wakita, Y. Itaya, Y. Yoshikuni, H. Asahi, *Electron. Lett.* **1986**, 22, 242.
- [7] N. Margalit, C. Xiang, S. M. Bowers, A. Bjorlin, R. Blum, J. E. Bowers, *Appl. Phys. Lett.* **2021**, 118, 220501.
- [8] S. Shekhar, W. Bogaerts, L. Chrostowski, J. E. Bowers, M. Hochberg, R. Soref, B. J. Shastri, *Nat. Commun.* **2024**, 15, 751.
- [9] W. Luo, L. Cao, Y. Shi, L. Wan, H. Zhang, S. Li, G. Chen, Y. Li, S. Li, Y. Wang, S. Sun, M. F. Karim, H. Cai, L. C. Kwek, A. Q. Liu, *Light: Sci. Appl.* **2023**, 12, 175.
- [10] P. Dong, Y.-K. Chen, G.-H. Duan, D. T. Neilson, *Nanophotonics* **2014**, 3, 215.
- [11] L. D. Marinis, N. Andrioli, G. Contestabile, *IEEE J. Select. Top. Quant. Electron.* **2023**, 29, 6.
- [12] M. Kamata, T. Baba, *Opt. Express* **2023**, 3115, 25245.
- [13] X. Zhang, K. Kwon, J. Henriksson, J. Luo, M. C. Wu, *Nature* **2022**, 603, 253.
- [14] F. Dell'Olio, J. Su, T. Huser, V. Sottile, L. E. Cortés-Hernández, C. Alix-Panabières, *Laser Photon. Rev.* **2021**, 15, 2000255.
- [15] S. Sun, B. Wang, K. Liu, M. W. Harrington, F. Tabatabaei, R. Liu, J. Wang, S. Hanifi, J. S. Morgan, M. Jahanbozorgi, Z. Yang, S. M. Bowers, P. A. Morton, K. D. Nelson, A. Beling, D. J. Blumenthal, X. Yi, *Nature* **2024**, <https://doi.org/10.1038/s41586-024-07057-0>.
- [16] F. Dell'Olio, T. Natale, Y.-C. Wang, Y.-J. Hung, *IEEE Sens. J.* **2023**, 23, 29948.
- [17] C. Yao, M. Chen, T. Yan, L. Ming, Q. Cheng, R. Penty, *Light: Sci. Appl.* **2023**, 12, 156.
- [18] Z. Xiao, W. Liu, S. Xu, J. Zhou, Z. Ren, C. Lee, *Adv. Opt. Mater.* **2023**, 20, 2301028.
- [19] C. Xiang, W. Jin, D. Huang, M. A. Tran, J. Guo, Y. Wan, W. Xie, G. Kurczveil, A. M. Netherton, D. Liang, H. Rong, J. E. Bowers, *IEEE J. Select. Top. Quant. Electron.* **2022**, 28, 1.
- [20] Y. Han, H. Park, J. Bowers, K. M. Lau, *Adv. Opt. Photonics* **2022**, 14, 404.
- [21] C. Xiang, W. Jin, J. E. Bowers, *Photonics Res.* **2022**, 10, A82.
- [22] S. Ghosh, S. Yegnanarayanan, D. Kharas, M. Ricci, J. J. Plant, P. W. Juodawlkis, *Opt. Express* **2023**, 31, 12005.
- [23] M. Churaev, R. N. Wang, A. Riedhauser, V. Snigirev, T. Blésin, C. Möhl, M. H. Anderson, A. Siddharth, Y. Popoff, U. Drechsler, D. Caimi, S. Hönl, J. Riemensberger, J. Liu, P. Seidler, T. J. Kippenberg, *Nat. Commun.* **2023**, 14, 3499.
- [24] M. J. R. Heck, J. F. Bauters, M. L. Davenport, D. T. Spencer, J. E. Bowers, *Laser Photonics Rev.* **2014**, 8, 667.
- [25] G. Z. Mashanovich, G. T. Reed, B. D. Timotijevic, S. P. Chan, in *Silicon Photonics*, 1 ed. (Ed: G. T. Reed), Wiley, Hoboken, NJ **2008**, pp. 15–46.
- [26] Y. Su, Y. Zhang, C. Qiu, X. Guo, L. Sun, *Adv. Mater. Technol.* **2020**, 5, 1901153.
- [27] J. F. Bauters, M. J. R. Heck, D. John, D. Dai, M.-C. Tien, J. S. Barton, A. Leinse, R. G. Heideman, D. J. Blumenthal, J. E. Bowers, *Opt. Express* **2011**, 19, 3163.

- [28] J. F. Bauters, M. J. R. Heck, D. D. John, J. S. Barton, C. M. Bruinink, A. Leinse, R. G. Heideman, D. J. Blumenthal, J. E. Bowers, *Opt. Express* **2011**, 19, 24090.
- [29] M. W. Puckett, K. Liu, N. Chauhan, Q. Zhao, N. Jin, H. Cheng, J. Wu, R. O. Behunin, P. T. Rakich, K. D. Nelson, D. J. Blumenthal, *Nat. Commun.* **2021**, 12, 934.
- [30] F. Dell'Olio, C. Ciminelli, M. N. Armenise, F. M. Soares, W. Rehbein, in *2012 International Conference on Indium Phosphide and Related Materials*, IEEE, Santa Barbara, CA, USA **2012**, pp. 124–127, <https://doi.org/10.1109/ICIPRM.2012.6403336>.
- [31] F. Dell'Olio, C. Ciminelli, M. N. Armenise, *Opt. Eng.* **2013**, 52, 024601.
- [32] P. Sibson, C. Erven, M. Godfrey, S. Miki, T. Yamashita, M. Fujiwara, M. Sasaki, H. Terai, M. G. Tanner, C. M. Natarajan, R. H. Hadfield, J. L. O'Brien, M. G. Thompson, *Nat. Commun.* **2017**, 8, 13984.
- [33] C. R. Pollock, M. Lipson, in *Integrated Photonics* (Eds: C. R. Pollock, M. Lipson), Springer US, Boston, MA **2003**, pp. 165–207.
- [34] A. Yariv, *Introduction to Optical Electronics*, Holt, Rinehart and Winston, New York **1976**.
- [35] L. Chrostowski, M. Hochberg, *Silicon Photonics Design*, Cambridge University Press, Cambridge **2015**.
- [36] W. Bogaerts, L. Chrostowski, *Laser Photonics Rev.* **2018**, 12, 1700237.
- [37] K. S. Kunz, R. J. Luebbers, *The Finite Difference Time Domain Method for Electromagnetics*, CRC Press, Boca Raton **1993**.
- [38] K. Yee, *IEEE Trans. Antennas Propagation* **1966**, 14, 02.
- [39] B. Rahman, J. Davies, *IEEE Trans. Microwave Theory Tech.* **1984**, 32, 20.
- [40] J. P. Webb, *Rep. Prog. Phys.* **1995**, 58, 1673.
- [41] D. F. G. Gallagher, T. P. Felici, in *Integrated Optoelectronics Devices* (Eds: Y. S. Sidorin, A. Tervonen) San Jose, CA **2003**, p. 69, <https://doi.org/10.1117/12.473173>.
- [42] W. Huang, C. Xu, S.-T. Chu, S. Chaudhuri, *J. Lightwave Technol.* **1992**, 10, 295.
- [43] C. Vassallo, *Opt. Quant. Electron.* **1997**, 29, 95.
- [44] J.-P. Berenger, *J. Comput. Phys.* **1994**, 114, 185.
- [45] C.-C. Huang, C.-C. Huang, J.-Y. Yang, *IEEE J. Select. Top. Quant. Electron.* **2005**, 11, 457.
- [46] C.-C. Huang, *Opt. Express* **2010**, 18, 26583.
- [47] A. Said, S. Obayya, *Opt. Quant. Electron.* **2023**, 55, 1027.
- [48] K. S. Chiang, *Opt. Quant. Electron.* **1994**, 26, S113.
- [49] Z. Zhu, T. G. Brown, *Opt. Express* **2002**, 10, 853.
- [50] C.-P. Yu, H.-C. Chang, *Opt. Express* **2004**, 12, 6165.
- [51] J. Lu, J. Vučković, *Opt. Express* **2013**, 21, 13351.
- [52] M. Paulsen, L. T. Neustock, S. Jahns, J. Adam, M. Gerken, *Opt. Quant. Electron.* **2017**, 49, 107.
- [53] E. Jaberansary, T. M. Masaud, M. M. Milosevic, M. Nedeljkovic, G. Z. Mashanovich, H. M. Chong, *IEEE Photonics J.* **2013**, 5, 3.
- [54] S. Hughes, L. Ramunno, J. F. Young, J. E. Sipe, *Phys. Rev. Lett.* **2005**, 94, 033903.
- [55] D. Melati, A. Melloni, F. Morichetti, *Adv. Opt. Photonics* **2014**, 6, 156.
- [56] Y. Shi, Y. Zhang, Y. Wan, Y. Yu, Y. Zhang, X. Hu, X. Xiao, H. Xu, L. Zhang, B. Pan, *Photonics Res.* **2022**, 10, A106.
- [57] D. J. Blumenthal, R. Heideman, D. Geuzebroek, A. Leinse, C. Roeloffzen, *Proc. IEEE* **2018**, 106, 2209.
- [58] D. Marcuse, *Theory of Dielectric Optical Waveguides*, 2 ed., Academic Press, Cambridge, MA **1991**.
- [59] A. W. Snyder, J. D. Love, *Optical Waveguide Theory*, Springer US, Boston, MA **1984**.
- [60] D. Marcuse, R. M. Derosier, *Bell Syst. Tech. J.* **1969**, 48, 3217.
- [61] N. R. Hill, *Phys. Rev. B* **1981**, 24, 7112.
- [62] S. G. Johnson, M. Ibanescu, M. A. Skorobogatiy, O. Weisberg, J. D. Joannopoulos, Y. Fink, *Phys. Rev. E* **2002**, 65, 066611.
- [63] D. Marcuse, *Bell Syst. Tech. J.* **1969**, 48, 3187.
- [64] A. W. Snyder, R. A. Sammut, *Electron. Lett.* **1979**, 15, 4.
- [65] A. W. Snyder, *JOSA* **1972**, 62, 1267.
- [66] D. Marcuse, *Bell Syst. Tech. J.* **1973**, 52, 817.
- [67] T. E. T. E. Murphy, *Design, Fabrication and Measurement of Integrated Bragg Grating Optical Filters*, Thesis, Massachusetts Institute of Technology **2001**.
- [68] A. Sudbo, *J. Lightwave Technol.* **1992**, 10, 418.
- [69] A. Snyder, *IEEE Trans. Microwave Theory Tech.* **1970**, 18, 608.
- [70] D. Marcuse, *Appl. Opt.* **1975**, 14, 3021.
- [71] I. A. White, A. W. Snyder, *Appl. Opt.* **1977**, 16, 1470.
- [72] A. Snyder, *IEEE Trans. Microwave Theory Tech.* **1969**, 17, 1138.
- [73] E. G. Rawson, *Appl. Opt.* **1974**, 13, 2370.
- [74] J. P. R. Lacey, F. P. Payne, *IEE Proc. J.* **1990**, 137, 282.
- [75] T. Barwicz, H. Haus, *J. Lightwave Technol.* **2005**, 23, 2719.
- [76] J. H. Schmid, A. Delâge, B. Lamontagne, J. Lapointe, S. Janz, P. Cheben, A. Densmore, P. Waldron, D.-X. Xu, K. P. Yap, *Opt. Lett.* **2008**, 33, 1479.
- [77] B. Guiana, A. Zadehghol, *Electronics* **2022**, 11, 307.
- [78] F. P. Payne, J. P. Lacey, *Opt. Quant. Electron.* **1994**, 26, 977.
- [79] C. Ciminelli, F. Dell'Olio, V. M. Passaro, M. N. Armenise, *Opt. Quant. Electron.* **2009**, 41, 285.
- [80] G. Pandraud, E. Margallo-Balbas, C.-K. Yang, P. J. French, *J. Lightwave Technol.* **2011**, 29, 744.
- [81] O. Fursenko, J. Bauer, A. Knopf, S. Marschmeyer, L. Zimmermann, G. Winzer, *Mater. Sci. Eng. B* **2012**, 177, 750.
- [82] M. Gehl, N. Boynton, C. Dallo, A. Pomerene, A. Starbuck, D. Hood, D. C. Trotter, A. Lentine, C. T. DeRose, *Opt. Express* **2018**, 26, 18082.
- [83] M. Grayson, B. Xu, T. Shanavas, M. Zohrabi, K. Bae, J. T. Gopinath, W. Park, *Opt. Express* **2022**, 30, 31107.
- [84] K. Inoue, D. Plumwongrot, N. Nishiyama, S. Sakamoto, H. Enomoto, S. Tamura, T. Maruyama, S. Arai, *Jpn. J. Appl. Phys.* **2009**, 48, 030208.
- [85] T. Horikawa, D. Shimura, T. Mogami, *MRS Commun.* **2016**, 6, 9.
- [86] C. Bellegarde, E. Pargon, C. Sciancalepore, C. Petit-Etienne, V. Hugues, D. Robin-Brosse, J.-M. Hartmann, P. Lyan, *IEEE Photonics Technol. Lett.* **2018**, 30, 591.
- [87] Y. Shi, L. Ma, Y. Zhuang, Z. He, *Opt. Express* **2020**, 28, 38733.
- [88] K. K. Lee, D. R. Lim, H.-C. Luan, A. Agarwal, J. Foresi, L. C. Kimerling, *Appl. Phys. Lett.* **2000**, 77, 1617.
- [89] J. Shin, Y.-C. Chang, N. Dagli, *Opt. Express* **2009**, 17, 3390.
- [90] A. Zadehghol, *IEEE Access: Pract. Innov. Open Solut.* **2021**, 9, 92326.
- [91] K. P. Yap, A. Delâge, J. Lapointe, B. Lamontagne, J. H. Schmid, P. Waldron, S. Janz, B. A. Syrett, *J. Lightwave Technol.* **2009**, 27, 3999.
- [92] R. G. Hunsperger, *Integrated Optics*, Springer, Berlin **1975**.
- [93] C.-L. Chen, *Foundations for Guided-Wave Optics*, John Wiley & Sons, Inc., Hoboken, NJ **2006**.
- [94] D. Melati, F. Morichetti, A. Melloni, *J. Opt.* **2014**, 16, 055502.
- [95] C. Kim, B. Jung, C. Lee, *Electron. Lett.* **1986**, 22, 296.
- [96] W.-Q. Peng, Y.-L. Wu, Y. Liu, Z.-Q. Yin, *J. Central South Univ.* **2012**, 19, 5 1317.
- [97] M. J. Adams, *An Introduction to Optical Waveguides*, Wiley, Hoboken, NJ **1981**.
- [98] C. G. Poulton, C. Koos, M. Fujii, A. Pfrang, T. Schimmel, J. Leuthold, W. Freude, *IEEE J. Select. Top. Quant. Electron.* **2006**, 12, 1306.
- [99] M. Reed, T. M. Benson, P. Sewell, P. C. Kendall, G. M. Berry, S. V. Dewar, *Opt. Quant. Electron.* **1996**, 28, 1175.
- [100] Z. H. Wang, *IEEE J. Quant. Electron.* **1998**, 34, 680.
- [101] D. Lenz, D. Erni, W. Bächtold, *Opt. Express* **2004**, 12, 1150.
- [102] W. C. Chew, J. S. Zhao, T. J. Cui, *Microwave Opt. Technol. Lett.* **2001**, 31, 252.
- [103] J. E. Sipe, *J. Opt. Soc. Am. B* **1987**, 4, 481.
- [104] K. A. Michalski, *Encyclopedia of RF and Microwave Engineering*, John Wiley & Sons, Ltd, Hoboken, NJ **2005**.

- [105] C. M. de Sterke, J. E. Sipe, *JOSA A* **1990**, 7, 636.
- [106] J. E. Goell, *Bell Syst. Tech. J.* **1969**, 48, 2133.
- [107] D. Marcuse, *Theory of Dielectric Optical Waveguides*, Elsevier, Amsterdam **2013**.
- [108] A. Hardy, W. Streifer, *J. Lightwave Technol.* **1985**, 3, 1135.
- [109] A. Yariv, *IEEE J. Quant. Electron.* **1973**, 9, 919.
- [110] C. Vassallo, *J. Lightwave Technol.* **1988**, 6, 294.
- [111] I. Papakonstantinou, R. James, D. R. Selviah, *J. Lightwave Technol.* **2009**, 27, 4151.
- [112] C. Ciminelli, V. M. N. Passaro, F. Dell'Olio, M. N. Armenise, *J. Eur. Opt. Soc. – Rap. Pub.* **2009**, 4, <https://doi.org/10.2971/jeos.2009.09015>.
- [113] C. Ciminelli, in *EOS Topical Meeting-Photonic Devices in Space*, Paris **2006**, pp. 18–19.
- [114] S. M. Hörmann, J. W. Hinum-Wagner, A. Bergmann, *J. Lightwave Technol.* **2023**, 41, 1503.
- [115] S. M. Hörmann, G. Feigl, J. W. Hinum-Wagner, A. Bergmann, *IEEE Photonics J.* **2024**, 16, 1.
- [116] S. M. Hörmann, J. W. Hinum-Wagner, A. Bergmann, in *Optical Modeling and Performance Predictions XIII*, SPIE **2023**, Vol. 12664, pp. 64–70, <https://doi.org/10.1117/12.2677385>.
- [117] J. W. Hinum-Wagner, S. M. Hoermann, J. Sattelkow, A. Buchberger, C. Schörner, S. Janka, G. Rossbach, D. Rist, J. Kraft, A. Bergmann, in *Optical Modeling and Performance Predictions XIII*, SPIE **2023**, Vol. 12664, pp. 28, <https://doi.org/10.1117/12.2677328>.
- [118] E. N. Fokoua, S. A. Mousavi, G. T. Jasion, D. J. Richardson, F. Poletti, *Adv. Opt. Photonics* **2023**, 15, 1.
- [119] H. Zhang, T. Li, A. Jian, S. Sang, C. Xue, W. Zhang, *Opt. Eng.* **2015**, 54, 125101.
- [120] D. M. Kita, J. Michon, S. G. Johnson, J. Hu, *Optica* **2018**, 5, 1046.
- [121] S. G. Johnson, P. Bienstman, M. A. Skorobogatiy, M. Ibanescu, E. Lidorikis, J. D. Joannopoulos, *Phys. Rev. E – Stat. Phys. Plasmas Fluids Related Interdisc. Top.* **2002**, 66, 15.
- [122] G. C. Righini, A. Chiappini, *Opt. Eng.* **2014**, 53, 071819.
- [123] S. Y. Siew, B. Li, F. Gao, H. Y. Zheng, W. Zhang, P. Guo, S. W. Xie, A. Song, B. Dong, L. W. Luo, C. Li, X. Luo, G. Q. Lo, *J. Lightwave Technol.* **2021**, 39, 4374.
- [124] A. Reisinger, *Appl. Opt.* **1973**, 12, 1015.
- [125] N. Frateschi, A. De Castro, *IEEE J. Quant. Electron.* **1986**, 22, 12.
- [126] R. E. Collin, *Foundations for Microwave Engineering*, Wiley, Hoboken, NJ **2001**.
- [127] Á. Barreda, F. Vitale, A. E. Minovich, C. Ronning, I. Staude, *Adv. Photonics Res.* **2022**, 3, 2100286.
- [128] F. Ladouceur, L. Poladian, *Opt. Lett.* **1996**, 21, 1833.
- [129] F. Morichetti, A. Canciamilla, C. Ferrari, M. Torregiani, A. Melloni, M. Martinelli, *Phys. Rev. Lett.* **2010**, 104, 3.
- [130] B. Peng, J. Rosenberg, W. D. Sacher, A. S. Jensen, M. Khater, W. M. J. Green, T. Barwicz, *Opt. Express* **2017**, 25, 23477.
- [131] F. Morichetti, A. Canciamilla, M. Martinelli, A. Samarelli, R. M. De La Rue, M. Sorel, A. Melloni, *Appl. Phys. Lett.* **2010**, 96, 081112.
- [132] B. J. Soller, D. K. Gifford, M. S. Wolfe, M. E. Froggatt, *Opt. Express* **2005**, 13, 666.
- [133] F. Morichetti, A. Melloni, A. Breda, A. Canciamilla, C. Ferrari, M. Martinelli, *Opt. Express* **2007**, 15, 17273.
- [134] E. Kleijn, P. J. Williams, N. D. Whitbread, M. J. Wale, M. K. Smit, X. J. M. Leijtens, *Opt. Express* **2012**, 20, 22660.
- [135] D. Melati, F. Morichetti, A. Canciamilla, D. Roncelli, F. M. Soares, A. Bakker, A. Melloni, *J. Lightwave Technol.* **2012**, 30, 3610.
- [136] A. Canciamilla, M. Torregiani, C. Ferrari, F. Morichetti, R. M. De La Rue, A. Samarelli, M. Sorel, A. Melloni, *J. Opt.* **2010**, 12, 104008.
- [137] W. Bogaerts, P. de Heyn, T. van Vaerenbergh, K. de Vos, S. Kumar Selvaraja, T. Claes, P. Dumon, P. Bienstman, D. van Thourhout, R. Baets, *Laser Photonics Rev.* **2012**, 6, 47.
- [138] A. Li, T. Van Vaerenbergh, P. De Heyn, P. Bienstman, W. Bogaerts, *Laser Photonics Rev.* **2016**, 10, 420.
- [139] F. Grillot, L. Vivien, S. Laval, E. Cassan, *J. Lightwave Technol.* **2006**, 24, 891.
- [140] G. Guerra, S. M. A. Mousavi, A. Taranta, E. N. Fokoua, M. Santagiustina, A. Galtarossa, F. Poletti, L. Palmieri, *J. Lightwave Technol.* **2022**, 40, 4714.
- [141] T. G. Nguyen, A. Boes, A. Mitchell, *IEEE J. Select. Top. Quant. Electron.* **2020**, 26, 1.
- [142] B. Rahman, J. Davies, *J. Lightwave Technol.* **1988**, 6, 52.
- [143] K. Morimoto, Y. Tsuji, *IEEE J. Quant. Electron.* **2019**, 55, 1.
- [144] V. Lombardi, M. Bozzi, L. Perregini, *IEEE Microw. Wireless Compon. Lett.* **2019**, 29, 631.
- [145] D. Marcuse, *Bell Syst. Tech. J.* **1970**, 49, 273.
- [146] G. Eleftheriades, A. Omar, L. Katehi, G. Rebeiz, *IEEE Trans. Microw. Theory Tech.* **1994**, 42, 1896.
- [147] W. A. Gambling, H. Matsumura, C. M. Ragdale, *Electron. Lett.* **1978**, 14, 130.
- [148] M. Heiblum, J. Harris, *IEEE J. Quant. Electron.* **1975**, 11, 75.
- [149] B. M. A. Rahman, D. M. H. Leung, S. S. A. Obayya, K. T. V. Grattan, *Appl. Opt.* **2008**, 47, 2961.
- [150] I. Papakonstantinou, K. Wang, D. R. Selviah, F. A. Fernández, *Opt. Express* **2007**, 15, 669.
- [151] J. P. N. Torres, V. M. Machado, A. Baptista, *IEEE Photonics J.* **2020**, 12, 1.
- [152] A. W. Snyder, I. White, D. J. Mitchell, *Electron. Lett.* **1975**, 11, 332.
- [153] I. A. White, *IEEE J. Microw. Opt. Acoust.* **1979**, 3, 186.
- [154] T. Chen, H. Lee, J. Li, K. J. Vahala, *Opt. Express* **2012**, 20, 22819.
- [155] F. Ladouceur, J. Love, T. Senden, *Optoelectron. IEE Proc.* **1994**, 141, 242.
- [156] T. Barwicz, H. I. Smith, *J. Vac. Sci. Technol. B: Microelectron. Nanometer Struct. Process. Meas. Phenom.* **2003**, 21, 2892.
- [157] F. Grillot, L. Vivien, S. Laval, D. Pascal, E. Cassan, *IEEE Photonics Technol. Lett.* **2004**, 16, 1661.
- [158] C. Qiu, Z. Sheng, H. Li, W. Liu, L. Li, A. Pang, A. Wu, X. Wang, S. Zou, F. Gan, *J. Lightwave Technol.* **2014**, 32, 2303.
- [159] L. Megalini, R. Shenoy, K. Rose, J. P. Speck, J. E. Bowers, S. Nakamura, D. A. Cohen, S. P. DenBaars, *Phys. Status Solidi A* **2016**, 213, 953.
- [160] M. S. Ab-Rahman, F. S. Ater, R. Mohamed, *Opt. Eng.* **2015**, 54, 055103.
- [161] D. E. Hagan, A. P. Knights, *J. Opt.* **2016**, 19, 025801.
- [162] K. Miarabbas Kiani, D. B. Bonneville, A. P. Knights, J. D. B. Bradley, *Appl. Sci.* **2022**, 12, 1363.
- [163] K. K. Lee, D. R. Lim, L. C. Kimerling, J. Shin, F. Cerrina, *Opt. Lett.* **2001**, 26, 1888.
- [164] S. Choi, K. Djordjev, Z. Peng, Q. Yang, S. J. Choi, P. Dapkus, *IEEE Photonics Technol. Lett.* **2004**, 16, 2266.
- [165] K. P. Yap, J. Lapointe, B. Lamontagne, A. Delâge, A. Bogdanov, S. Janz, B. Syrett, in *Device and Process Technologies for Microelectronics, MEMS, Photonics, and Nanotechnology IV*, Vol. 6800, SPIE **2008**, pp. 259–270, <https://doi.org/10.1117/12.758968>.
- [166] L. Ottaviano, M. Pu, E. Semenova, K. Yvind, *Opt. Lett.* **2016**, 41, 3996.
- [167] M. Oliver, R. Webster, *CATENA* **2014**, 113, 56.
- [168] S. Bruzzone, M. Kaveh, *IEEE Trans. Acoust. Speech Signal Process.* **1984**, 32, 701.
- [169] L. S. J. Marple, *Digital Spectral Analysis: Second Edition*, Courier Dover Publications, Garden City, NY **2019**.
- [170] P. M. T. Broersen, *IEEE Trans. Instrum. Meas.* **2007**, 56, 1189, <https://doi.org/10.1109/TIM.2007.900418>.
- [171] M. B. Priestley, *Spectral Analysis and Time Series*, 3rd printing, Academic Press, London **1984**.
- [172] G. M. Jenkins, *J. R. Stat. Soc. Ser. C* **1965**, 14, 2.

- [173] J. Durbin, G. S. Watson, *Biometrika* **1950**, 37, 409.
- [174] P. M. T. Broersen, in *2006 IEEE Instrumentation and Measurement Technology Conference Proceedings* **2006**, pp. 868–873, <https://doi.org/10.1109/IMTC.2006.328236>.
- [175] C. J. W. Zorn, *Am. J. Pol. Sci.* **2001**, 45, 470.
- [176] R. Kan, X. Wang, *J. Econom.* **2010**, 154, 101.
- [177] D. B. Percival, A. T. Walden, *Spectral Analysis for Univariate Time Series*, Cambridge University Press, Cambridge **2020**.
- [178] J. R. M. Hosking, *J. Econom.* **1996**, 73, 261.
- [179] D. L. Zimmerman, M. B. Zimmerman, *Technometrics* **1991**, 33, 77.
- [180] C. Fleming, J. Calabrese, On the Estimators of Autocorrelation Model Parameters **2013**.
- [181] J. Huillery, F. Millioz, N. Martin, *IEEE Trans. Signal Process.* **2008**, 56, 2249.
- [182] C. E. Rasmussen, C. K. Williams, *Gaussian Processes for Machine Learning*, MIT Press, Cambridge, MA **2006**.
- [183] H. Liu, Y.-S. Ong, X. Shen, J. Cai, *IEEE Trans. Neural Netw. Learn. Syst.* **2020**, 31, 4405.
- [184] P. Whittle, *Hypothesis Testing in Time Series Analysis*, Ph.D. Thesis, University of Uppsala **1951**.
- [185] A. P. Guillaumin, A. M. Sykulski, S. C. Olhede, F. J. Simons, *J. R. Stat. Soc. Ser. B: Stat. Methodol.* **2022**, 84, 1526.
- [186] T. W. Anderson, *J. Time Ser. Anal.* **1997**, 18, 321.
- [187] M. A. Delgado, J. Hidalgo, C. Velasco, *Annals Stat.* **2005**, 33, 2568.
- [188] P. Preuss, M. Vetter, H. Dette, *Scand. J. Stat.* **2013**, 40, 417.
- [189] M. Sagmeister, G. Koppitsch, P. Muellner, S. Nevlacsil, A. MaeseNovo, R. Hainberger, D. Seyringer, J. Kraft, in *Proceedings of MDPI EUROSENSORS 2018*, Multidisciplinary Digital Publishing Institute **2018**, Vol. 2, p. 1023, <https://doi.org/10.3390/PROCEEDINGS2131023>.
- [190] J. Wang, M. M. Sanchez, Y. Yin, R. Herzer, L. Ma, O. G. Schmidt, *Adv. Mater. Technol.* **2020**, 5, 6.
- [191] A. Z. Subramanian, E. Ryckeboer, A. Dhakal, F. Peyskens, A. Malik, B. Kuyken, H. Zhao, S. Pathak, A. Ruocco, A. D. Groote, P. Wuytens, D. Martens, F. Leo, W. Xie, U. D. Dave, M. Muneeb, P. V. Dorpe, J. V. Campenhout, W. Bogaerts, P. Bienstman, N. L. Thomas, D. V. Thourhout, Z. Hens, G. Roelkens, R. Baets, *Photonics Res.* **2015**, 3, B47.
- [192] A. Buchberger, J. Pulko, D. Morecroft, O. Basso, J. Kraft, A. Bergmann, in *Conference on Lasers and Electro-Optics. In Conference on Lasers and Electro-Optics*, OSA, Washington, D.C. **2021**, p. JTh3A.84, https://doi.org/10.1364/CLEO_AT.2021.JTh3A.84.
- [193] F. Vogelbacher, S. Nevlacsil, M. Sagmeister, J. Kraft, K. Unterrainer, R. Hainberger, *Opt. Express* **2019**, 27, 31394.
- [194] X. Ji, J. K. Jang, U. D. Dave, M. Corato-Zanarella, C. Joshi, A. L. Gaeta, M. Lipson, *Laser Photonics Rev.* **2021**, 15, 2000353.
- [195] C. Ciminelli, F. Dell'Olio, M. N. Armenise, F. M. Soares, W. Passenberg, *Opt. Express* **2013**, 21, 556.
- [196] Q. Du, Y. Huang, J. Li, D. Kita, J. Michon, H. Lin, L. Li, S. Novak, K. Richardson, W. Zhang, J. Hu, *Opt. Lett.* **2016**, 41, 3090.
- [197] P. Ma, D.-Y. Choi, Y. Yu, X. Gai, Z. Yang, S. Debbarma, S. Madden, B. Luther-Davies, *Opt. Express* **2013**, 21, 29927.
- [198] K. B. Yoon, *Macromol. Res.* **2004**, 12, 474.
- [199] H. Li, Y. Anugrah, S. J. Koester, M. Li, *Appl. Phys. Lett.* **2012**, 101, 111110.
- [200] Y. Yang, J. Wu, X. Xu, Y. Liang, S. T. Chu, B. E. Little, R. Morandotti, B. Jia, D. J. Moss, *APL Photonics* **2018**, 3, 120803.
- [201] S. Park, J. J. Ju, J. T. Kim, M.-S. Kim, S. K. Park, J.-M. Lee, W.-J. Lee, M.-H. Lee, *Opt. Express* **2009**, 17, 697.
- [202] L. Cai, A. Mahmoud, G. Piazza, *Opt. Express* **2019**, 27, 9794.
- [203] R. G. Hunsperger, *Integrated Optics*, Springer New York, New York, NY **2009**.
- [204] U. Glombitza, E. Brinkmeyer, *J. Lightwave Technol.* **1993**, 11, 1377.
- [205] A. Peczek, C. Mai, G. Winzer, L. Zimmermann, in *2020 IEEE 33rd International Conference on Microelectronic Test Structures (ICMTS)*, IEEE, Edinburgh, UK **2020**, pp. 1–3, <https://doi.org/10.1109/ICMTS48187.2020.9107905>.
- [206] H. Shoman, H. Jayatileka, N. A. F. Jaeger, S. Shekhar, L. Chrostowski, *Opt. Express* **2020**, 28, 10225.
- [207] G. T. Reed, A. P. Knights, *Silicon Photonics: An Introduction*, 1st ed., Wiley, Hoboken, NJ **2004**.
- [208] R. Regener, W. Sohler, *Appl. Phys. B: Photophys. Laser Chem.* **1985**, 36, 143.
- [209] R. Adar, Y. Shani, C. H. Henry, R. C. Kistler, G. E. Blonder, N. A. Olsson, *Appl. Phys. Lett.* **1991**, 58, 444.
- [210] R. Adar, M. Serbin, V. Mizrahi, *J. Lightwave Technol.* **1994**, 12, 1369.
- [211] M. Popović, *Theory and Design of High-Index-Contrast Microphotonic Circuits*, Thesis, Massachusetts Institute of Technology **2008**.
- [212] Q. Deng, L. Liu, X. Li, J. Michel, Z. Zhou, *Opt. Lett.* **2016**, 41, 4747.
- [213] M. A. Tran, T. Komljenovic, J. C. Hulme, M. L. Davenport, J. E. Bowers, *IEEE Photonics Technol. Lett.* **2016**, 28, 1517.
- [214] Y. A. Vlasov, S. J. McNab, *Opt. Express* **2004**, 12, 1622.
- [215] T. Feuchter, C. Thirstrup, *IEEE Photonics Technol. Lett.* **1994**, 6, 1244.
- [216] E. D. Palik, *Handbook of Optical Constants of Solids*, Academic Press, Cambridge, MA **1998**.
- [217] P. Dong, W. Qian, S. Liao, H. Liang, C.-C. Kung, N.-N. Feng, R. Shafiiha, J. Fong, D. Feng, A. V. Krishnamoorthy, M. Asghari, *Opt. Express* **2010**, 18, 14474.
- [218] C. G. Roeloffzen, M. Hoekman, E. J. Klein, L. S. Wevers, R. B. Timens, D. Marchenko, D. Geskus, R. Dekker, A. Alippi, R. Grootjans, A. Van Rees, R. M. Oldenbeuving, J. P. Epping, R. G. Heideman, K. Worhoff, A. Leinse, D. Geuzebroek, E. Schreuder, P. W. Van Dijk, I. Visscher, C. Taddei, Y. Fan, C. Taballione, Y. Liu, D. Marpaung, L. Zhuang, M. Benelajla, K. J. Boller, *IEEE J. Select. Top. Quant. Electron.* **2018**, 24, 4.
- [219] A. Chanana, H. Larocque, R. Moreira, J. Carolan, B. Guha, E. G. Melo, V. Anant, J. Song, D. Englund, D. J. Blumenthal, K. Srinivasan, M. Davanco, *Nat. Commun.* **2022**, 13, 7693.
- [220] S. Gundavarapu, M. Belt, T. A. Huffman, M. A. Tran, T. Komljenovic, J. E. Bowers, D. J. Blumenthal, *J. Lightwave Technol.* **2018**, 36, 1185.



Francesco Dell'Olio received the M.S. degree in electronic engineering and the Ph.D. degree in 2005 and 2010, respectively. He is an associate professor at the Department of Electrical and Information Engineering, Polytechnic University of Bari, Italy. He has been involved in several research projects funded by Italian Ministry of University and Research, European Space Agency, Italian Space Agency, and industrial companies, some of which involved taking on the role of a Principal Investigator. His research interests include silicon photonics and nanophotonics, with particular regard to modeling, design, and characterization of devices and integrated circuits for telecommunications, microwave photonics, and sensing.



Samuel M. Hörmann is a Ph.D. candidate at Graz University of Technology and formerly with ams OSRAM Group. His research focuses on modeling of surface-roughness-induced scattering. He combines perturbation theory with statistically motivated spectral analysis of two-dimensional roughness to achieve predictive modeling of fabrication-induced imperfections. By integrating these methods into holistic design workflows, his work aims to balance sensitivity and optical loss for integrated photonic sensors. His broader interests include the interplay between numerical modeling and experimental validation to enhance the performance and reliability of photonic platforms for sensing and communication applications.



Teresa Natale was born in 1998. She received the M.S. degree in electronic engineering from the Polytechnic University of Bari, Bari, Italy, in 2022, where she is currently pursuing the Ph.D. degree in electrical and information engineering. Her M.S. thesis was partially carried out at the Physics Department, Biomolecular Photonics Laboratory, University of Bielefeld, Bielefeld, Germany. Her research is focused on silicon photonics, microphotonics, and nanophotonics with a specific focus on applications related to inertial sensing.